Modeling and Analysis of a Maneuvering Aircraft and Cable Towed Body with Wake Effects

by

Jacob Thomas Hall

B.S., United States Air Force Academy (2008)

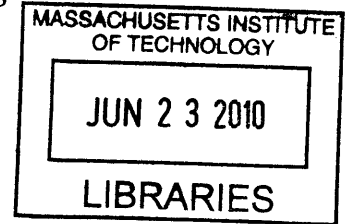Submitted to the Department of Aeronautical and Astronautical Engineering
in partial fulfillment of the requirements for the degree of

Master of Science in Aeronautical and Astronautical Engineering

at the

MASSACHUSETTS INSTITUTE OF TECHNOLOGY

June 2010

Author...
Department of Aeronautical and Astronautical Engineering
May 7, 2010

Certified by......................
Jaume Peraire
Professor of Aeronautics and Astronautics
Thesis Supervisor

Certified by............................
Eric Burcsu
Technical Staff, MIT Lincoln Laboratory
Thesis Supervisor

Accepted by...........
Eytan H. Modiano
Associate Professor of Aeronautics and Astronautics
Chair, Committee on Graduate Students

Modeling and Analysis of a Maneuvering Aircraft and Cable Towed Body with Wake Effects

by

Jacob Thomas Hall

Submitted to the Department of Aeronautical and Astronautical Engineering
on May 7, 2010, in partial fulfillment of the
requirements for the degree of
Master of Science in Aeronautical and Astronautical Engineering

Abstract

This thesis report covers the analysis and modeling of a cable towed endbody that incorporates an aircraft, wake effects, a towline, and a tow body. The aircraft is modeled as a generic tactical aircraft which is able to conduct maneuvers. The towline is treated as an elastic cable that connects the aircraft and endbody while also being affected by the aircraft wake. The endbody is treated as a simple drag sphere with allocation to continue to various shapes and sizes. A parametric study is conducted which highlights the effect of changing the parameters of towline material, length, and load factor. Three maneuvers are conducted including a turn and acceleration. The results show that longer cable lengths, those of $500\,m$ or greater, exhibit little response to the addition of a trailing wake. However, shorter cables are affected, especially during the turn and climb maneuvers. A $50\,m$ cable experiences an extra $8\,m$ deflection when compared to a wake-less example. During the climb maneuver, it is shown that an endbody may pass ahead of the towing aircraft, as well as above it. The effect of changing cable material is shown to be minimal, with small differences expected due to the difference in cable mass.

Thesis Supervisor: Jaume Peraire
Title: Professor of Aeronautics and Astronautics

Thesis Supervisor: Eric Burcsu
Title: Technical Staff, MIT Lincoln Laboratory

Acknowledgements

I would like to thank many people in helping me accomplish this thesis project. First of all, my wife and family for always supporting me in my adventures prior to and during my assignment to graduate school at MIT. Without their love and support, I don't think I would have completed this thesis, let alone made it through MIT classes and my undergraduate experience at USAFA. Second of all, I would like to thank my Lincoln Laboratory advisor, Eric Burcsu. Eric has been a staff member for Group 109 (formerly 49) for quite sometime, and his daily help and guidance was essential in completing this thesis as well as navigating a path through graduate school. This thesis project would not haven been possible without his help and expertise. I would also like to thank all of the other staff members of Group 109, as well as associate staff, assistant staff, secretaries, and especially the graphics department in answering oddball questions on everything from the proper use of Fortran and Bluemax to the process of ordering a research article from the Lincoln Laboratory archives.

I also thank the Air Force Rapid Capabilities Office in sponsoring my graduate studies at MIT and research. Also, I am thankful for MIT Lincoln Laboratory providing space, advisors, as well as a project for this thesis research. Lastly, I would like to thank my on campus MIT advisor, Professor Jaume Peraire, in contributing to the thesis project and laying out the MIT guidelines. His vast knowledge of the aerodynamics involved as well as the modeling of wake vortices were great resources in completing this project.

Disclaimer

The views expressed in this article are those of the author and do not reflect the official policy or position of the United States Air Force, Department of Defense, or the U.S. Government.

Contents

List of Figures

11

List of Tables

Chapter 1

Introduction

The cable towed endbody system has various applications across many fields of science and engineering. The system appears in all aspects of engineering, as well as in general day to day experiences. The cable towed endbody system appears in an ocean environment, where tugboats tow massive ships and speedboats tow water skiers. It also appears underwater, where ships tow sensors and submarines tow various payloads on very long cables. The system also appears in the air where aircraft tow gliders, sensors, decoys, and even scientific instruments. The cable towed endbody system also represents the motion of helicopters carrying supplies or armaments when they are sling-loaded beneath the aircraft. It even appears in space applications, where space shuttles can be used to deploy tethered satellites or other payloads. These are just a few of the systems that rely on the idea of one object towing another through the use of a strong and flexible cable. Each case represents unique challenges in regards to their equations of motion, simplifying assumptions, and their operating environments.

Cable towed endbodies appear in a broad area of applications across all environments. In each situation, the system is subject to different parameters, assumptions, and motions but the underlying principles apply to all. For example, the underwater towed array of a submarine is subject to a buoyant force, while an aircraft towed glider produces lift, and a water-skier is subject to friction between the ski's and water surface. The cable used by a water-skier is most likely more flexible than a

much stronger cable towed by a tugboat. The endbody parameters also differ, as a sling-loaded truck beneath a helicopter exhibits more drag than a decoy trailing behind an aircraft. The broad base of application means that it has been heavily researched over the years, however, new technologies and world situations continue to uncover priority research areas. In this thesis, one application of the cable towed endbody system is investigated, however, the findings and modeling methodology maybe applied to a much broader subject area given different simplifying assumptions and environments. The more specific area motivating this thesis is the cable towed aerial decoy.

Ever since aircraft were first used for combat in World War I, various inventions have been made to deny them the advantage of the "high ground". As technology has increased through the years following 1914, these inventions have evolved from high caliber shells to missiles flying more than three times the speed of sound. Along with the technological growth in means to bring down aircraft, a similar growth in protection measures has evolved. Today, aircraft rely on things such as stealth, electronic countermeasures, chaff, flares, and aerially towed decoys to survive in hostile environments.

All methods have been tested and proven in combat, each with their advantages and disadvantages. Stealth aircraft rely on expensive materials and aircraft design to make the aircraft appear nearly invisible to radar, thus avoiding enemy airplanes and surface-to-air missiles. Electronic countermeasures comprise of sophisticated electronics and technology to confuse or jam enemy weapons and radars, rendering them useless. Chaff and flares are inexpensive, expendable decoys that rely on little technology to attract and disorient enemy missiles; however, new technologies allow missiles to discern between them and the intended target.

Advances in research have led to the development of more technical decoys that rely on more sophisticated technology to defeat enemy attacks. These are known as aerially towed decoys, which are relatively inexpensive, when compared to the cost of losing a pilot and plane. The decoys work with minimal inputs from an already overburdened pilot to lure enemy missiles away from an aircraft. They are also more

16

Figure 1-1: Modern Towed Decoy[24]

technologically advanced then chaff and flares, with the ability to actively lure an incoming missile away. All of the protection measures mentioned are used in todays modern air combat. This research will focus solely on the aerially towed decoy, an evolving invention that has yet to reach its peak technologically.

1.1 Basics

The purpose of the towed decoy system is to enable the aircraft to survive an encounter with an enemy air-to-air or surface-to-air missile. This allows aircraft to operate in hostile environments. A towed decoy system is comprised of three parts. The first part is the towing aircraft, usually a tactical aircraft. The United States, as well as many countries around the globe, employ towed decoys to protect aircraft. The aircraft carries the decoy in a pod, usually underneath a wing, from which it is released to the rear of the aircraft during flight.

The aircraft is attached to the decoy through the second main part, the towline. Various towline lengths, materials, and areas are used in the world and therefore these are treated as parameters in this study. The towline design is very important, as it must strike a balance between strength and flexibility while minimizing drag in order to keep the decoy attached during all forms of flight.

17

Most decoys are aerodynamically shaped objects which remain in the free stream following the towing aircraft. The majority of decoys incorporate drag fins to enhance stabilization as well as to keep the decoy located behind the aircraft. When deployed, the decoy presents a target for enemy missiles that is hopefully more attractive than the towing aircraft itself. Different models of decoys employ different tactics in defeating enemy missiles, however, they all have the same goal of luring any missile away from the more valuable aircraft.

1.2 Research Focus

Decoys have been used for decades, however, questions still remain about certain aspects of their use, as well as the cable towed endbody system itself. The dynamical response of the system when subjected to aircraft maneuvers and the resulting aircraft wake field is the focus of this study. Tactical aircraft employ decoys in a high threat environment, which is associated with combat maneuvers such as high-G turns and loops. Not only is the decoy subjected to the tension from the cable during these maneuvers, but also the strong wake vortices that are present following an aircraft.

In the event of an enemy missile attack, the decoy may not be located directly behind the tactical aircraft following such maneuvers, and may or may not prove effective at luring missiles in different positions and orientations. This study is conducted to determine the response of the towed-decoy system during maneuvers over varied cable parameters. The decoy position, cable shape, as well as system level responses to maneuvers are a few of the items to be examined and analyzed. The actual effectiveness of the decoy in performing its mission is beyond the scope of this study.

The common shortfalls that exist in the current research dealing with aerially towed objects include limitation to steady, simple flight and disregarding the wake produced by the aircraft. During high-G maneuvers, the wakes produced by the aircraft are very complex and powerful. The wake may even remain at a great distance from an endbody unless the maneuver brings the decoy through the resultant wake

vortices. However, the towline near the aircraft attachment point will most likely experience disrupted flow, and its effects will translate down the towline to affect the endbody response. Maneuvers coupled with the associated aircraft wake may affect the effectiveness of an aerially towed decoy, and the goal of this study is to provide the groundwork for such research.

Another common shortfall is the assumption of an inextensible towline. Many authors choose not to analyze the towline as an extensible object because it adds time and computational requirements. They also reason that most towlines are made of steel, or other high modulus materials that don't strain easily. Because the combined effects of wake and maneuvers on a towed-decoy system are unknown, this thesis report will treat the towline as extensible in order to analyze all aspects of the system. Due to modern advances in modeling and analysis, the application of an extensible cable is no longer a major hindrance.

1.3   Objectives

In order to study the important dynamics of such a system, a cable-endbody model is constructed. This model includes a generic tactical aircraft, an extensible towline, and a simple drag sphere acting as an endbody that is affected by aerodynamic forces, wake vortex induced velocities, as well as aircraft maneuvers. The model is subjected to steady, straight flight, as well as maneuvering flight, and its results are compared to other researcher's results.

Various maneuvers, such as high-G turns, are studied and modeled, and their resulting wake fields are created. The models are based on a generic tactical combat aircraft. The wakefield created during the maneuvers is approximated using a pair of vortex filaments. It is a simplified wake field, as it assumes that the wake rolls up and this can be approximated by only two trailing wake vortices. The towed endbody system is taken through those maneuvers and their resulting wake to analyze its response by means of position, orientation, shape, and tension. The reactions of the system to the maneuvers and resulting wakes are important to understand endbody

19

dynamics in realistic environments.

1.4 Layout

This thesis will first cover the background and historical research on the area of cable towed decoys, as well as other applications of the cable towed endbody system. Each researcher contributed in some manner to the research done today and their main efforts will be highlighted. They are organized into the main portions of the system, including endbodies, cable dynamics, maneuvers, and their associated wake fields. Next, the thesis will show how the system is modeled. The fundamental mathematical equations as well as assumptions will be presented to provide a starting point for other interested researchers.

After finalizing the model implementation with a section on wake modeling, the thesis will present comparisons to other models created in the past. These older models' results were digitally re-scaled and imported into Matlab in order to compare. The comparison models are chosen to test the steady state, dynamic state, and parameter variation in order to highlight any differences in expected response. Some differences are to be expected, as will be explained for each researcher has made different assumptions.

Following the comparison chapter will be the results and analysis. It includes the assessment of two assumptions made in the modeling, the time step and activity distance of the segmented trailing wake vortices. It also includes results and analysis of the system during maneuvers. The system is placed in steady, level turns, as well as more aggressive turns. The effects of changing parameters of length, cable material, wake, as well as load factor are examined. Other maneuvers are covered including a climb.

In the last section of the thesis, conclusions are drawn along with laying out a path ahead in research. The conclusions focus on things learned from the application of wakes as well as the general approach in modeling. The recommendations for future research will include topics that can build on this research, interesting results

that should be investigated further, as well as ideas that may enhance the system for future use.

Chapter 2

Literature Review

2.1 Groundwork

The dynamics of a towed body system have been studied since the early 1900s. During the early years, the focus was on towing balloons and gliders[7]. Glauert led the English Aeronautical Research Committee in research on cable shapes while pulling heavy loads in level flight. The results would be very timely, because following his initial research in the mid 1930's, towed gliders were used frequently in World War II. They were essential in ferrying troops across the English Channel during the D-Day invasion at Normandy. Glauert's work laid the foundation for most cable-towed endbody studies in the future.

One of his main contributions includes the assumption that most of the cable drag occurs from the normal component of the incoming wind, which other authors would coin as the cross-flow model of drag around cylinders[8]. This assumption simplifies the aerodynamic forces encountered by the cable and allows for easier computation. He notes, however, that "the assumption is a very close approximation to the actual experimental results unless the angle ϕ is very small," which is the angle measured vertically between the aircraft and the endbody[7]. At certain speeds, or with certain endbodies, this assumption will not apply. Glauert's analysis of the cable in per unit length characteristics, dividing the cable into segments, also simplifies the cable system and is followed by many researchers thereafter.

2.2 Endbodies

Glauert's early work dealt mainly with the cable's dynamics, and because the research was sound, it allowed researchers to work on other aspects of the towed body system. Research during and following the 1960s and 1970s then began to focus on various types of endbodies. These included things such as targets, which Pierce and Beecham delve into[20]. Their work is very important in the area of towing objects at supersonic speeds.

At the time, researchers were interested in the ability of missiles to intercept supersonic targets. In order to flight test, the targets were towed by aircraft up to supersonic speeds, where drag on the cable and its affects on the target endbody had not been analyzed. Pierce and Beecham developed a method for calculating tension and drag as it is distributed along the cable during supersonic flight using supersonic wind-tunnels and various diameter wires. Their results show that cable skin friction, as well as the turbulent boundary layer, play a part in the cable dynamics at supersonic speeds, both of which are usually assumed to be negligible in the subsonic regime.

Another area of research which appears in this time frame is the analysis of sling loads[17]. It may appear to be a completely different area, considering it involves helicopters and heavy loads such as artillery pieces or trucks, but sling loading dynamics is also very similar to cable towed decoy dynamics. Nagabhushan and Cliff find that instabilities will occur in translational and rotational motion with the sling loads. These instabilities can cause unwanted oscillatory motion that is undamped and exponentially diverging which should be avoided for safe flight. The main parameters to monitor to avoid such instabilities are reported as tow body to vehicle mass ratio, tow cable length, and load factor during a turn.

The authors also find that a low sling load to aircraft mass ratio is favorable to stability during maneuvers. At higher load factors the divergence in helicopter motion also increases. If the sling load mass is high compared to the aircraft, a stability augmentation system may prove valuable to aid a pilot already overburdened with

24

other tasks. These important parameters, such as length and load factor are also analyzed in this report, as they impact the reactions and stability of the towed cable endbody system.

Also, in the 1960's, researchers focused on the dynamics of magnetic anomaly detectors (MAD) [14], which are instruments used to find and track submarines that are towed on a cable by a patrol plane. Interested in a complete analysis of the airborne towed vehicle system, Lehn et al. modeled and flight tested, the system in various conditions and subject to different parameters. They discover there exists an envelope in which the cable towed system remains stable despite translational or rotational maneuvers. Their analysis centers on a single cable length of 250 ft and a single airspeed of 150 $KTAS$. They find that disturbances at the tow aircraft are repeated by the MAD sensor with a time lag of around a half of a second in this environment.

In the same area of tracking submarines, ship towed decoys and sonar arrays are also researched heavily during this era. Choo and Casarella provide important work in 1973 in which they survey the various analytical methods of simulating cable-body systems[2]. As they show, many of the methods used to analyze underwater towed bodies can also apply to aerially towed bodies. Choo and Casarella cover everything from the method of characteristics and rigid body dynamics to finite element methods. They find the best methodology depends upon the complexity of the system and environment modeled; for example, the finite element method presents the most versatile method but requires enormous computational time, whereas a simple two degree of freedom spring method can model basic issues with ease.

In the more modern era, endbodies appear that require more detailed approaches. Cochran and co-authors published research on one of these new endbodies, a fully maneuverable towed body in 1992[11]. Cochran and fellow researchers assumed an inextensible tow cable, however, they add to the area of research by developing a stability and control augmentation system for a maneuverable towed body. They present two methods of numerically solving the system, a Runge-Kutta fourth order method and an Euler method. Their work is used to develop a maneuverable towed target

which is the first to be flown above the towing aircraft and recovered successfully. Their results are important in understanding the complexity behind new endbodies which can do anything from maneuvering around the towplane to holding its course and altitude in spite of tow aircraft movement.

Tagging onto Cochran's research, Norris and Andrisani contribute by analyzing and comparing their model of a controllable cable towed aircraft for a space launch vehicle research to actual data[19]. NASA research flights were conducted in 1998 using a C-141 aircraft towing an F-106 aircraft; a highly loaded delta wing fighter plane simulating a future space launch vehicle. Norris and Andrisani use the results from these flight tests to compare with their own numerical results, showing that the equilibrium shape of the cable system relies heavily on the towed aircraft's flight path angle as well its elevator deflection angle. They note that in some trim conditions, the glider actually places itself ahead of the towplane given necessary cable length and system altitude.

2.3 Cable Dynamics

Other research during the time period focuses solely on the towing cable. Genin and various co-author's contributed greatly to the study of cable-towed endbodies and are pioneers in the area for the American engineers. Genin and Huffman show, in a 1970 report, that speed and cable length are the main determining factors for cable motion, and that the motion differs from simple pendulum oscillation in most cases[9]. Genin and Cannon, in research done for Purdue University, show that the component of cable drag in the tangential direction should not be assumed as a negligible effect as many previous researchers had[6]. Genin also finds that the cable density is more important than the attitude of the tow aircraft when finding the steady state shape of the towline. The densities they investigate include those associated with nylon and steel cables. They also contribute by reporting their modeling approach using the Runge-Kutta method, which simplifies modeling of the cable decoy system.

Later on, in 1979, Swedish researchers focused on detecting the allowable ac-

26

celerations of different towing vehicles, given the strength of the wire and various characteristics of the system[16]. This is important when the endbody is something such as a target, or glider, so the tow cable does not break during a maneuver. In the study, Matuk reports that the allowable accelerations are based upon the endbody mass, towline length, area, and the magnitude of acceleration. Since this study, most researchers have debated whether treating the cable portion of the system elastically is important or not. With improvements in numerical methods and computer speed, treating the cable elastically is no longer out of the question.

More modern research in cable dynamics is dominated by a few key players. One of these is Bernard Etkin, whose research into endbody instabilities and extensible cables is cited by many researchers thereafter. Etkin's contribution revolves around the stability of a towed body system with an extensible towline, and a generic towed mass subject to lift and drag[5]. His work shows that inherent instabilities with the system exist when the towline attachment is located at the center of gravity. This occurs only when the endbody is designed to provide lift or moments about its center of gravity other than the drag force.

This correlates with research done by Nakagawa and Obata, who show that the location of the attachment point is crucial in determining endbody stability as well as endbody stability derivatives[18]. More importantly, Etkin's method also shows that treating the towline elastically is possible, even while using relatively simple techniques in Matlab. He also reports that the elasticity of the cable isn't as important for shorter cables as it is for longer systems. Etkins studies, however, are focused only on the steady, straight and level flight, and their reactions to small perturbations.

Cable dynamics is also the topic of relatively recent research done at the Air Force Institute of Technology in 2006. Two researchers, Richardson and Hill, contributed Master's Theses under the guidance of Ralph Anthenien in the area of cable shape and position as well as jet plume effects to cable towed systems. Their research suggests that even ignoring the jet plume may present a problem to towed decoys.

Richardson's work focuses on modeling the dynamics of a cable towed decoy system and analyzing the results of various parametric sweeps[4]. He uses a fourth order

Runge-Kutta method within Matlab by employing the ode45 solver, which is also used in this thesis. He, however, assumes the cable is inextensible along with most other researchers despite what Etkin reports. He characterizes the cable shape for steady, level flight with two non-dimensional parameters. One is a body forces group, which is defined by the density of the cable, diameter of the cable, gravity, density of the air, and velocity shown in equation 2.1. The second is the decoy weight to drag ratio seen in equation 2.2.

$$\frac{\rho_t \pi d_t g}{2 \rho_a V^2} \tag{2.1}$$

$$\frac{W_d}{D_d} \tag{2.2}$$

Between these two groups of parameters, Richardson finds that all steady cable shapes of the cable and endbody can be determined. A lower value of the body forces group, lower than 0.025, indicates a more horizontal cable while values higher than 0.25 indicate a more vertical cable. The decoy weight to drag ratio also affects the cable shape, with values higher than 5 becoming more vertical, and values lower than 0.1 becoming more horizontal. Richardson determines these bounds in order to avoid two specific problems.

If the decoy and cable are too horizontal out the back of the aircraft, the jet plume may burn through the cable or at least sever communications between the endbody and aircraft, but if the shape is too vertical the decoy may drag along the ground or hit obstacles during low altitude maneuvers. Interesting to note, these parameter groups do not include length, which may not play a pivotal role in cable shape at least in the steady state situation. Richardson notes that length is still a parameter when the model is accelerated, thus, length is still investigated in the dynamic analysis found in this thesis.

2.4 Maneuvers

As some researchers delve into the intricate details of the cable, some others focus on applications of the cable. During the early 1980s, Karlsen reported on the dynamics

of a towed object system when subjected to maneuvers[12]. His research includes dynamical response to maneuvers such as turns and accelerations, which provides a basis for comparison to this thesis report. Karlsen's work focuses on extremely long towing cables, ranging from $2\,km$ to $5\,km$.

The properties he investigates include the cable shape, endbody location, as well as tension within the cable, all while conducting maneuvers. The scope of his research is somewhat limited, however, as he also assumes an inextensible towline and ignores wake effects on the cable. Karlsen notes on page 14 of his work, "For an accurate description of the tensile force in rapid transition maneuvers it is necessary to solve the longitudinal equations with elastic waves included." Given the assumptions, Karlsen's work is an excellent resource for comparison and many of his results are digitized and compared in Chapter 4.

Also compared in Chapter 4 is the work of Hill, who produced his AFIT thesis on this subject. Richardson's research laid the groundwork for Hill's approach, which focuses on dynamic cases of perturbations as well as heat transfer from the jet plume[3]. Hill creates a dynamic code in order to analyze small maneuvers and their affects on cable shape. He uses the method of characteristics to create the dynamic code, which is slightly less accurate than Richardson's use of a Runge-Kutta method, but provides similar results as seen on page 66 of his thesis. Hill also assumes the cable to be inextensible and limits maneuvers to small perturbations and accelerations.

He finds an acceptable way to model the heat transfer due to an aircraft's engine jet plume that can be included in the dynamic cable shape code. This is used to find hot spots or points where the cable is experiencing higher than average heat. Hill's research provides a first attempt at defining maneuvers that may affect the effectiveness of a cable towed decoy, as he shows a slight perturbation in the vertical direction may cause a cable to pass through the jet plume. This depends on the decoy and cable parameters, as shown by Richardson, but given the right conditions, the cable does experience a heat transfer due to the jet plume, and further modeling is needed to determine if the heat transferred is enough to melt the cable or sever communications between the aircraft and decoy.

More current in the area of maneuvers is the research done by Quisenberry and Arena. Their expertise includes actively controlled objects that are towed at low level and must remain at a certain altitude above the terrain[21]. Both the towing aircraft and the towed endbody are subjected to maneuvers. This research is important for ocean surveillance, where the towed object must stay above waves and their varying heights and adjust altitude using a pitching surface. It follows the research done by Cochran, as the object must actively maneuver in order to remain at a certain altitude given different motion from the towing aircraft. Quisenberry and Arena create models of ocean wave forms on top of creating a cable towed endbody model in order to integrate things such as wave height into a control equation.

They're detailed work includes an autopilot for the endbody which can take in altitude, wave height, and aerodynamic forces and output an action to servos in order to rotate wing angle on the endbody. They find the ability to maintain altitude depends almost entirely on the sample rate that the endbody's radar altimeter and accelerometer are set to. They also find that as the aircraft's altitude increases, the accuracy in which the towed body is following the general waveform also increases. The longer cable allows the endbody's autopilot to maneuver more precisely and stay just above the waves, while also allowing the endbody to correct for towing aircraft motions or disturbances. This set up allows the towing aircraft to operate at a safe altitude while still gathering meaningful data for their research.

Although the specific area of endbody research differs from the goal of this thesis, the math and analysis provided by Quisenberry and Arena are a great resource on how to use modern techniques in modeling and analyzing the cable endbody system. They report again in 2006 by analyzing the different discrete methods of cable modeling including lumped mass and thin rod approximations[22]. The majority of previous researchers had modeled the cable as a long connection of distinct lumped masses, where all forces are applied and evaluated. Quisenberry and Arena find this method, although very simple, requires small time-steps in numerical simulation in order to stay numerically stable. They show that modeling the cable as connected thin rods decreases the reliance on computation and despite requiring more work and

complexity up front in developing the equations of motion, leads to much quicker numerical solutions.

Increasing in complexity, researchers at the Royal Melbourne Institute of Technology invest heavily in the analysis of long flexible towlines connected to an orbiting aircraft[25]. This is the third modern area of research and it focuses on flying a towing cable in large circles and slowly lowering the tip all the way to the ground where it would remain theoretically motionless. Williams and partners have produced numerous articles describing the methodology in modeling such a system and creating control algorithms that would dictate the cable shape and length in order to accomplish said objective. They create a flexible, extensible, lumped mass model of a very long cable attached to an orbiting aircraft. They then subject the cable to drag, deployment forces, relative winds, as well as elevated terrain in order to analyze its usefulness in picking up stationary payloads off the ground and whisking them away.

Williams' main contribution to the area is the addition of a flexible and extensible cable, as a model had been created prior that didn't allow for the normal bowing and cable re-shaping due to things such as drag and winds aloft. He shows that it is possible to optimize the problem through controlling the cable length via a winch reel mechanism on the aircraft. This mechanism can control the amount of cable released. This application of towed cables could prove itself as an important technology in the future for things such as picking up payloads in hostile territory or maybe even retrieving soldiers behind enemy lines.

Williams' research group finds some interesting results, including the assessment that increased terrain height increases the cost of the operation. Cost is defined in terms of energy, as the reeling in and out of the cable at the aircraft requires more frequent and greater accelerations. They also find it is possible to conduct multiple pickups in the same general region with minimal changes at the aircraft while using only the control system. Interestingly, they find addition of gusting winds aids the control system when flying into the wind, whereas a tailwind detracts from the efficiency of the system. This is because the headwind increases drag on the cable, pushing it further behind the aircraft, therefore giving the control system more time

and cable length to optimize the pick up.

2.5   Wake

The fourth area of research in cable endbody analysis is relatively new and rich with research opportunities. One of these areas is researched by Zhu and Meguid, the modeling of aerial refueling. Although many Air Forces around the world have practiced aerial refueling for decades now, the modeling of the action has recently become more important. This focus area arose with the introduction and operation of unmanned aerial vehicles (UAV's) throughout the world's air forces. At the present time, many of these vehicles are really remotely piloted vehicles (RPV's), where they are flown by a human at a ground station by means of a communication link. Many of the newer UAV's, however, are looking to operate autonomously with minimal human input. In order to accomplish missions which manned aircraft can, it may be a requirement for them to aerially refuel automatically, thus the need for models of aerial refueling in order to write programs for UAV's to refuel.

Zhu and Meguid produced numerous papers on modeling the cable towed endbody system in a general sense[28] and in a specific application of refueling drogues[27][26]. They use a finite element method to model an aerial refueling drogue. This is an apparatus which drags behind a refueling aircraft attached by a long, rubber hose. The drogue transmits fuel to a needy aircraft via a probe which is attached to most Navy aircraft, as the Air Force uses a completely different method for its aircraft. The hose and drogue follow behind a tanker aircraft in its wake, and act similarly to a cable decoy system with a few different properties, such as hose material and size.

They model the system based on a finite element method using 3 node beam elements. Their approach is useful for complex systems or shapes but demands alot of computational resources, which is exacerbated by the thicker refueling hose compared to the width of a normal cable. They subject the cable model to small vertical displacements, as well as the wake induced velocity from the wingtips and refueling pod of a tanker aircraft. Zhu and Meguid's results show that any disturbance encountered

by the refueler aircraft will be amplified as it travels downstream and leads to hose whipping with an associated tension spike near the drogue, as much as seven times the steady state tension. This can cause premature refueling separation between the probe and drogue, as well as possible hose rupture. Both of these problems need to be avoided in order to safely refuel manned as well as unmanned aircraft. They also find that the hose and drogues reaction to the wake vortices generated by the aircraft depends upon the length of the hose. Shorter hoses, around 1.5 m, show a tendency to orbit around the vortex filament and may hit the trailing edge of the refueler's wing. Longer hoses orbit in a bow shape causing the drogue to move in small circles. In general, they find that as the length of the hose increases, the wake has less effect on the drogue, suggesting that a fast retrieval and deployment of the drogue system with long cables is needed in order to avoid the vortex orbiting motion of shorter hoses.

Zhu and Meguid's study is one of the more extensive studies to date and includes the wake effects of the towing aircraft. However, their study is limited to one application and a constant set of cable parameters. They also assume that the vorticity of the wake fields created by the aircraft are constant, and that the aircraft is only subjected to small disturbances. In this thesis, the towing aircraft will be maneuvering, therefore the vorticity will not be a constant, and the cable parameters will be varied. In order to apply the model to more than one specific situation, a finite difference approach will be taken instead of the more complex, time consuming, and computer resource intensive finite element method.

Chapter 3

Model

Modeling the aerially towed decoy is quite complicated due to the multitude of variables which affect its motion. The decoy itself is an aerodynamic body subject to drag and lift forces, which are sometimes augmented with drag or stabilization fins. It is tethered to a moving tactical aircraft by means of a cable. This cable also experiences lift and drag forces, as well as tension due to the endbody load and the aircraft pulling at opposing ends. The aircraft is also maneuvering over time, displacing the rest of the system which affects the tension and relative wind it encounters. Meanwhile, because of the maneuvers and motion of the system, the gravitational force, although constant, acts along different fixed axes along the cable and decoy.

3.1 Foundation

The following mathematical methods and simplifications are based on E.J. Kelly's process of modeling a cable towed endbody[13]. His work, produced in the latter part of the 1990's at MIT Lincoln Laboratory, is used as a reference for the steady state and dynamic equations of the cable system. Because Kelly's work is not widely available, the equations used in his approach are reprinted here, in sections 3.1 to 3.5. Kelly's extensive work lays out a path for representing a cable-endbody system, however, the actual modeling, as well as incorporating wake effects, aircraft maneuvers, and a detailed analysis are produced originally in this thesis.
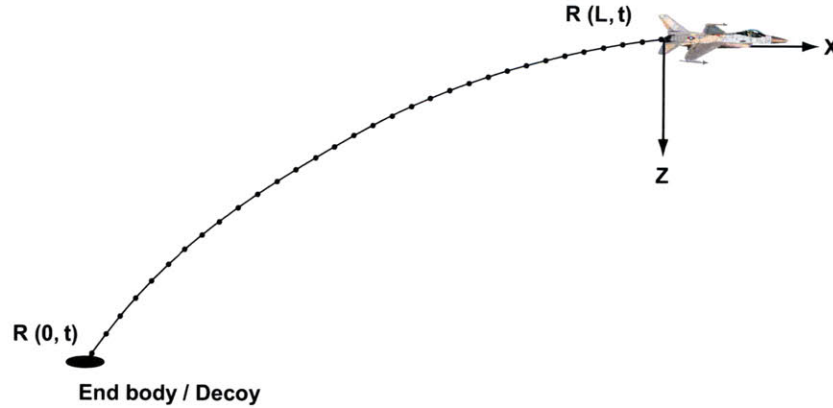
Figure 3-1: Coordinate System

The analysis begins by creating a stationary coordinate system whose origin is at the towplane attachment point of the cable and whose principal directions are x, y, and z. The positive x-direction is out the nose of the towplane, the y direction pointing right, parallel with the wing, and the z-direction is downwards to the earth. This origin is located at the initial timestep, before the aircraft has begun maneuvering. Positions of the cable and endbody will be based off of this origin.

The position of individual elements on the cable is then given by a vector, $\mathbf{R}(s,t)$. The variable s refers to the specific point along the cable, where the point at $s = 0$ corresponds to the endbody end of the cable, while $s = L$ is the end of the cable which is attached to the tactical aircraft, L being the total length of cable. The value of t corresponds to the time that has elapsed since the beginning of the maneuver. $\mathbf{R}(L, 0)$, therefore, is the origin of the reference frame, or the location of the towplane attachment point before the simulation has started. Expanded in the three principal directions of x,y,z, the vector is given by

$$\mathbf{R} = X(s,t)\mathbf{e}_x + Y(s,t)\mathbf{e}_y + Z(s,t)\mathbf{e}_z \qquad . \qquad (3.1)$$

Every point along the cable will be modeled across the time span, therefore the array $\mathbf{R}(s,t)$ stores most of the information which is vital to the primary goal of this research. Figure 3-1 shows the manner in which the inertial coordinate system is

created, as well as the positions along the cable.

3.2 Elastic Cable

The cable is treated as an extensible object, therefore, the effects of tension will be based on the strain experienced by each cable segment. The strain at the mid-point of each segment, e, is found by,

$$e(s,t) = |\frac{\partial \mathbf{R}(s,t)}{\partial s}| - 1 \qquad (3.2)$$

or, equivalently, $|\mathbf{R}'| - 1$. The tension, T, is calculated from the strain, e, using a simple Hooke's Law relation for our elastic material,

$$T = AEe \qquad , \qquad (3.3)$$

where A is the cable reference area and E is the cable's modulus of elasticity. The tension vector, $\mathbf{T}$, is found by multiplying the tension force, T, by the tangential unit vector,

$$\mathbf{T} = T\mathbf{t} = T\frac{\mathbf{R}'}{1 + e} \qquad . \qquad (3.4)$$

3.3 Non-Dimensionalization

The equations of motion are much more simplified in the non-dimensional form. Also, the inherent parameters which affect the variables and equations are much more visible. To non-dimensionalize, each parameter or variable which deals in units of length will be divided by the total cable length, L. Also, all values of mass will be divided by μL which is the mass per unit length of the cable multiplied by the total length, or the total cable mass. All force values are non-dimensionalized by dividing by cable area, A, and cable modulus, E. Velocities are non-dimensionalized using the cable wave speed, c_L. Finally, acceleration is non-dimensionalized by dividing the quantity by c_L^2/L. Non-dimensional quantities will be underlined to highlight the

difference with their original dimensional quantities. The equations above are now non-dimensionalized below, but first one must find the acual cable wave speed in order to non-dimensionalize velocities.

$$c_L = \sqrt{\frac{AE}{\mu}} \qquad . \tag{3.5}$$

The time is non-dimensionalized using the length of the cable L and its wave speed c_L which is given by,

$$t = \frac{L}{c_L}\underline{t} \qquad . \tag{3.6}$$

Therefore, the main values of interest are the placement along the cable, s, the position of the system elements, $\mathbf{R}$, and the tension T. These values are non-dimensionalized in the following equations.

$$s = L\underline{s} \qquad , \tag{3.7}$$

$$\mathbf{R}(s,t) = L\underline{\mathbf{R}}(\underline{s},\underline{t}) \qquad , \tag{3.8}$$

$$T = AE\underline{T} \qquad . \tag{3.9}$$

Strain is already a non-dimensional value, therefore, rearranging 3.3 shows that $\underline{T} = \underline{e}$. The tension vector equation is simplified by using the non-dimensional relationships of $\underline{a}$ and $\underline{b}$ which are given by,

$$\underline{a} = \frac{\underline{T}}{1 + \underline{e}} \tag{3.10}$$

$$\underline{b} = \frac{\underline{T}'}{1 + \underline{e}} - \underline{T}\frac{\underline{e}'}{(1 + \underline{e})^2} \qquad . \tag{3.11}$$

Therefore,

$$\underline{\mathbf{T}} = \underline{a}\,\underline{\mathbf{R}}' \qquad , \tag{3.12}$$

$$\underline{\mathbf{T}}' = \underline{a}\,\underline{\mathbf{R}}'' + \underline{b}\,\underline{\mathbf{R}}' \qquad . \tag{3.13}$$
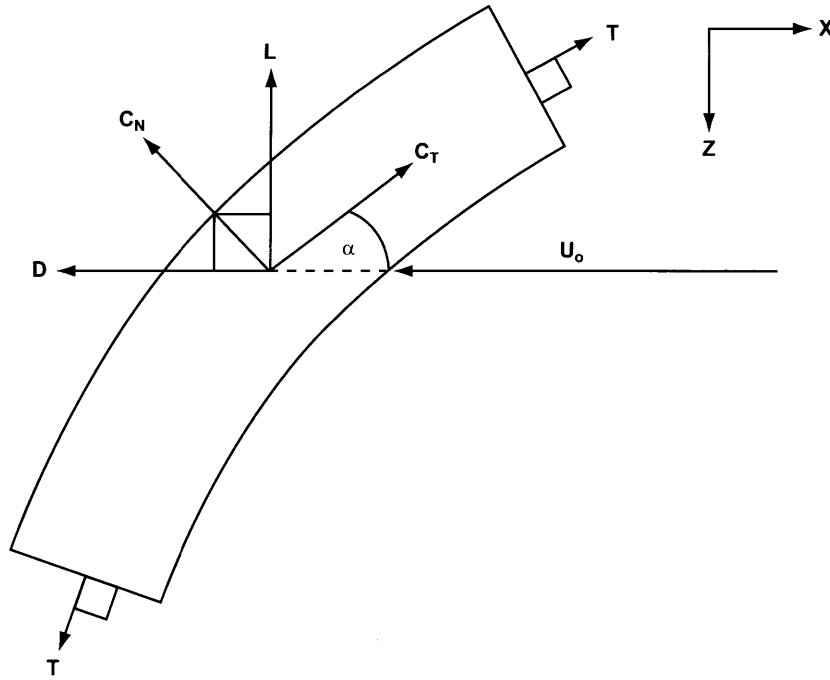
Figure 3-2: Forces Acting on Cable Segment

3.4 Equations of Motion

3.4.1 Cable

The cable motion is described in two equations[13]. The first relates the non-dimensionalized acceleration of a cable segment, $\ddot{\underline{R}}$, to the forces caused by gravity, tension, and the aerodynamics. Figure 3-2 details the forces which are applied on a cable segment of length ds. Those forces appear in that order in equation 3.14 and each are described in more detail below. The equation is essentially Newton's second law, $\sum F = m\,a$, rearranged and simplified for the forces the cable encounters. The second equation, 3.15, shows the relationship between strain and tension, which is simplified by using the Hooke's law model.

$$\ddot{\underline{R}} = \underline{\chi}\mathbf{e}_z + \underline{a}\,\mathbf{R}'' + \underline{b}\,\mathbf{R}' + \mathbf{f_a} \tag{3.14}$$

$$\underline{T} = \underline{e} \tag{3.15}$$

39

$\ddot{\mathbf{R}}$ is the non-dimensional acceleration vector for each point along the cable, s, at a specific time, t. $\underline{\chi}$ is a non-dimensional parameter which represents the gravitational force, and it is given by,

$$\underline{\chi} = \frac{\mu g L}{AE} \quad , \tag{3.16}$$

where μ is the mass per unit length of the cable, g is the acceleration due to gravity, L is the total length of the cable, A is the cross sectional cable area, and E is the cable's modulus of elasticity. The term $\underline{a}\,\mathbf{R}'' + \underline{b}\,\mathbf{R}'$ describes the tension experienced by the cable segment, as shown previously, the $\underline{a}$ and $\underline{b}$ values are used to simplify the equation's appearance.

The non-dimensional aerodynamic force encountered by the ds portion of the cable is represented by $\underline{\mathbf{f_a}}$. This force depends on the angle of attack, normal and tangential aerodynamic forces, and the relative wind seen by the cable segment. The angle of attack is calculated with knowledge of the cable tangential unit vector, $\mathbf{t}$, and the apparent wind unit vector, $\mathbf{e_w}$. The tangential unit vector is found using the magnitude of the tension and its force vector seen in equations 3.3 and 3.4. The apparent wind vector is found through the vector addition of system airspeed and cable velocity.

$$\underline{\mathbf{W}} = \underline{u_0} + \dot{\mathbf{R}} \tag{3.17}$$

The value $\underline{u_0}$ is the non-dimensionalized flow speed which can be found by dividing the flow velocity U_0 by the wave propagation speed along the cable c_L,

$$\underline{u_0} = \frac{U_0}{c_L} \quad . \tag{3.18}$$

The apparent wind unit vector is then given by,

$$\mathbf{e_w} = \frac{\underline{\mathbf{W}}}{\underline{W}} = \frac{1}{\underline{W}}(\underline{u_0} + \dot{\mathbf{R}}) \quad . \tag{3.19}$$

Therefore the angle of attack is defined by,

$$cos\,\alpha = \mathbf{e_w} \cdot \mathbf{t} \quad . \tag{3.20}$$

The dimensionalized version of the aerodynamic force is found through a simple cross-flow model which is used by previous researchers,

$$\mathbf{f_a} = (1 + e)qD[C_n(\alpha)\mathbf{N} - C_t(\alpha)\mathbf{t}] \qquad , \qquad (3.21)$$

where e is the strain, q is the dynamic pressure, and D is the cable diameter. C_n is a normal cable drag function applied in the normal direction $\mathbf{N}$, dependent on the angle of attack, α, while C_t is the tangential cable drag function applied in the tangential direction $\mathbf{t}$. The normal cable drag function determines the normal drag coefficient and it is described by the following function,

$$C_n(\alpha) = \underline{C_n}(\alpha) = \underline{c_n}sin(\alpha) \qquad , \qquad (3.22)$$

where $\underline{c_n}$ is a specified normal force cable drag coefficient. Likewise, the tangential cable drag function is defined using a specified tangential drag coefficient $\underline{c_t}$,

$$C_t(\alpha) = \underline{C_t}(\alpha) = \underline{c_t}cos(\alpha)|cos(\alpha)| - \underline{c_n}sin(\alpha)cos(\alpha) \qquad . \qquad (3.23)$$

These normal and tangential functions vary between different researchers, along with the coefficients, so they were chosen following Kelly's mathematical process [13]. The non-dimensionalized version of equation 3.21 is found by dividing by the cable area, A, and modulus E while also multiplying by the cable length L. The extra multiplication is needed because the analysis is conducted in segments of cable ds where the force is found per unit length. This also provides reasoning for the $(1 + e)$ term, as the cable segment length is actually $(1 + e)ds$ in an extensible cable.

$$\underline{\mathbf{f_a}} = -(1 + \underline{e})\underline{\eta_c}\underline{W}^2[\underline{C_n}(\alpha)\mathbf{N} - \underline{C_t}(\alpha)\mathbf{t}] \qquad . \qquad (3.24)$$

The constant $\underline{\eta_c}$ is a non-dimensional coefficient that is used to simplify constants

41

found in the aerodynamic force function, it is,

$$\underline{\eta_c} = \frac{\rho D L}{2\mu} \quad , \tag{3.25}$$

which as shown depends on the air density, cable diameter, cable length, and mass per unit length of the cable. This is only possible because of the manner in which the relative wind is non-dimensionalized, like all other velocities, by cable wave speed,

$$\underline{W} = \frac{W}{c_L} \quad . \tag{3.26}$$

3.4.2 Endbody

A separate non-dimensionalized equation of motion is needed for the endbody as it reacts in a slightly different manner than a standard cable segment. Very similar to the cable, the endbody's equation of motion is described as

$$\ddot{\underline{\mathbf{R}}} = \underline{\chi}\mathbf{e}_z + \frac{1}{R_M}(\underline{a}\,\underline{\mathbf{R}}' + \underline{\mathbf{F_a}}) \quad . \tag{3.27}$$

It can also be found by rearranging Newton's second law, as the acceleration $\ddot{\underline{\mathbf{R}}}$ is set equal to the sum of the forces on the endbody including gravity, tension from the cable attachment, and the aerodynamic force, all divided by mass. The first term is the same term described earlier, the gravitational force defined by the non-dimensional parameter $\underline{\chi}$. The second, $\underline{R_M}$, is the non-dimensionalized mass of the endbody,

$$\underline{R_M} = \frac{M}{\mu L} \quad . \tag{3.28}$$

The third term, $\underline{a}\,\underline{\mathbf{R}}'$, is the tension force on the endbody due to its attachment to the last cable segment. The last term is the non-dimensional aerodynamic force, which differs from the cable's aerodynamic force. Dimensionalized, it is found through the following equation with knowledge of the coefficient of drag, $\underline{C_{D0}}$, the constants of air density, ρ, reference area, S_r, the magnitude of relative wind, W, and the wind

42

vector, $\mathbf{W}$.

$$\mathbf{F_a} = -\frac{1}{2}\rho\underline{C_{D0}}S_r W\mathbf{W} \tag{3.29}$$

Non-dimensionalizing the aerodynamic force is conducted by dividing out the cable area, A, and the cable modulus, E.

$$\underline{\mathbf{F_a}} = -\frac{\rho C_{D0}S_r}{2AE}W\mathbf{W} = -\frac{\rho C_{D0}S_r}{2\mu}\underline{W}\mathbf{W} \tag{3.30}$$

Knowing that the relative wind is a combination of cable motion and airspeed, as shown in equation 3.17, leads to our endbody aerodynamic non-dimensionalized force given by the following.

$$\underline{\mathbf{F_a}} = -\underline{\eta_e}\underline{C_{D0}}\underline{W}(\underline{u_0} + \dot{\underline{\mathbf{R}}}) \tag{3.31}$$

The term $\underline{\eta_e}$ is a non-dimensional parameter which simplifies the equation by combining the constants of air density, ρ, reference area, S_r, and non-dimensionalizing mass per unit length μ,

$$\underline{\eta_e} = \frac{\rho S_r}{2\mu} \qquad . \tag{3.32}$$

3.5   Solution Process

3.5.1   Boundary Conditions

The first step in the solution process is defining the boundary conditions. The boundaries are determined by two separate objects, the aircraft and the endbody. The bottom of the cable is attached to the endbody. The reaction of the endbody to the current aerodynamic environment will define the boundary of the cable at the bottom ($s = 0$) end. Reference the previous section for the equations which detail the motion of the endbody, as it is somewhat different then a cable segment's equation of motion.

In order to simplify the towed-decoy system, the endbody is originally treated as a drag sphere. In essence, it is an object with a given weight, coefficient of drag, and moments of inertia which allows the cable to exhibit tension and compression. The drag sphere is easily replaced by more complicated endbodies that can represent

43

anything from a modern decoy to the refueling drogue of a tanker aircraft.

These more complicated shapes will react differently with the cable and aircraft depending on their weight, coefficients of drag and lift, as well as their moments of inertia. Forces on the endbody, regardless of shape or construction, will also affect the rest of the cable, creating waves along the extensible cable which will interact with waves created by the aircraft end of the cable.

The second boundary condition is defined by the actions of the aircraft. The very top of the cable, which is attached to the towplane, has a position defined by the motion of the towing aircraft

$$\underline{\mathbf{R}}(\underline{L}, \underline{t}) = \underline{\mathbf{R}}_{a/c} \qquad . \qquad (3.33)$$

Initially, the towplane motion will be in steady, level flight. This will be used to find a steady state position of the cable that each combat maneuver analyzed will begin from. After a brief time of steady flight, $2 - 5 \ km$, the aircraft will then execute a specified maneuver, and re-reach a new steady state. The maneuvers in this thesis were generated using a generic flight simulator used by the Air Force and MIT Lincoln Laboratory. Any flight simulation program may be used, as long as the necessary output can be obtained. The position of the aircraft and as its velocities over time are recorded and used in the dynamic solution process described later in this chapter as they are the states associated with the top cable segment. The aircraft orientation and load factor are also recorded, as these variables affect the release point and strength of the trailing wake, which will also be detailed later.

Using a flight simulation program can be avoided all together if one can create column vectors for each necessary aircraft variable for each required timestep during the maneuver. Many initial runs were conducted using straight flight by the aircraft for a specific period of time, thereby simplifying all of the required aircraft states and enabling a user to create a maneuver without a simulation by applying the laws of kinematics.

44

3.5.2 Steady State

The next step in the solution process is computing the steady state position of the cable when subjected to parameters such as airspeed and altitude. From the steady state solution, one can then find the dynamic response of the system over time using a finite difference scheme. This same scheme can be used by the steady state solver with simplification as the acceleration and time terms fall out of the equations, as the cable remains unaccelerated and unchanged over time in a steady state.

The solution process starts by discretizing the time and spatial parameters of the cables position,

$$\underline{s}_n = n\delta\underline{s} \qquad , \tag{3.34}$$

$$\underline{t}_m = m\delta\underline{t} \qquad . \tag{3.35}$$

Because the initial goal is solving the steady state shape of the cable endbody system, the time index is at first disregarded. The process begins by implementing a finite difference scheme in a Matlab M-file. The finite difference equations are used to solve for the unaccelerated state of the cable using a function in Matlab called Fsolve. Fsolve is a nonlinear system solver that computes the vector $\mathbf{x}$ in a problem defined by $F(\mathbf{x}) = 0$. The solver is supplied with an initial guess at the solution vector $\mathbf{x}$ and it returns a converged vector solution following an iterative process which drives the residual to zero. It conducts this process using one of a few chosen algorithms but defaults to the trust region dogleg method. This method drives the current value of $F(\mathbf{x})$ to zero by analyzing the derivatives and determining which values of $\mathbf{x}$ should be increased or decreased. This iterative process is continued until the residual is zero, or within the tolerance specified by the user.

In our case, the $\mathbf{x}$ vector contains the coordinates of each cable segment, while the function $F(\mathbf{x})$ calculates the acceleration of each cable segment. The acceleration of each segment is found by first using a set of simplified finite difference equations. The equations below are used to find the strain in each cable segment. Once again, it is important to note that while solving for the steady state cable, the time terms, or

the indices of m are disregarded as the steady state position is unchanged over time.

$$\underline{\mathbf{R}}''[n, m] = \frac{1}{\delta \underline{s}^2}(\underline{\mathbf{R}}[n + 1, m] - 2\underline{\mathbf{R}}[n, m] + \underline{\mathbf{R}}[n - 1, m]) \tag{3.36}$$

$$\underline{\mathbf{R}}'[n, m] = \frac{1}{2\delta \underline{s}}(\underline{\mathbf{R}}[n + 1, m] - \underline{\mathbf{R}}[n - 1, m]) \tag{3.37}$$

The two main finite difference equations above are used to find the strain on the interior cable segments using equations 3.10 through 3.13. The cable segments that attach to the endbody and aircraft rely on forward and backwards differences as shown in the next two equations.

$$\underline{\mathbf{R}}'_+[n, m] = \frac{1}{\delta \underline{s}}(\underline{\mathbf{R}}[n + 1, m] - \underline{\mathbf{R}}[n, m]) \tag{3.38}$$

$$\underline{\mathbf{R}}'_-[n, m] = \frac{1}{\delta \underline{s}}(\underline{\mathbf{R}}[n, m] - \underline{\mathbf{R}}[n - 1, m]) \tag{3.39}$$

These forward and backward differences combine with the following forward and difference approximations to calculate strain at the two cable attachment points.

$$\underline{e}_+[n, m] = |\underline{\mathbf{R}}'_+[n, m]| - 1 \tag{3.40}$$

$$\underline{e}_-[n, m] = |\underline{\mathbf{R}}'_-[n, m]| - 1 \tag{3.41}$$

This strain, along with the calculated aerodynamic and gravitational forces on each segment from equations 3.24 and 3.16 are used to find the acceleration of the cable segments in equation 3.14, while the endbody acceleration is found using its equation of motion in equation 3.27. The accelerations are compiled into a vector, $F(\mathbf{x})$, which the Fsolve function drives to zero by altering the $\mathbf{x}$ vector containing the positions of each cable segment.

3.5.3 Dynamic State

Once the steady state position of the cable is computed, it is used to start the dynamic solution process. The overall goal of the dynamic solver is to produce a state vector

Table 3.1: System States and State Derivatives

Number	State	Derivative
$1-3$	Endbody Position (x,y,z) m	Endbody Velocity (x,y,z) m/s
$4-6$	Endbody Velocity (x,y,z) m/s	Endbody Acceleration (x,y,z) m/s^2
$7-9$	Endbody Moments (L,M,N) $m*s$	Endbody Rotation Rates (P,Q,R) m/s
$10-13$	Endbody Quaternions (q0,q1,q2,q3)	Endbody Quaternion Rates $(\dot{q}0, \dot{q}1, \dot{q}2, \dot{q}3)$ $1/s$
$14-n+14$	Cable Segments X Position m	Cable Segments X Velocity m/s
$n+15-2n+15$	Cable Segments Y Position m	Cable Segments Y Velocity m/s
$2n+16-3n+16$	Cable Segments Z Position m	Cable Segments Z Velocity m/s
$3n+17-4n+17$	Cable Segments X Velocity m/s	Cable Segments X Acceleration m/s^2
$4n+18-5n+18$	Cable Segments X Velocity m/s	Cable Segments X Acceleration m/s^2
$5n+19-6n+19$	Cable Segments X Velocity m/s	Cable Segments X Acceleration m/s^2

containing important information about the system throughout the specified system motion. The states are found in Table 3.1 with their associated derivatives. The derivatives are important, because they are assembled in a separate Matlab M-file and solved over the timespan using another Matlab solver, ode45. This ordinary differential equation solver uses initial state values and creates its own time steps to solve the state values over a given time span. The solver is supplied the derivatives of the state vector, and it produces the state vector through a Runge-Kutta integration method. In the equation $\mathbf{y}' = f(t, \mathbf{y})$, the solver is given the derivatives, vector $\mathbf{y}'$ and integrates to find the states found in vector $\mathbf{y}$.

The basic states begin with the position, velocity, and quaternion orientation of the endbody. The position and velocity of the cable segments are also states, as well as the the position and velocity of the aircraft. Because the position and velocity of the aircraft are supplied by the flight simulation output, these states do not need to be solved but are included for the sake of organization. Using the state vector approach simplifies the solution process as nearly half of the derivatives are given already by the previous states. The solver, ode45, takes in the previous time-step's states each time it is compiling the state derivatives. For example, to solve for the derivative of the cable position, one may use the cable's velocity which is already a part of the state vector. The derivatives which aren't apart of the state vector, such as the acceleration of the cable, are solved for using a finite difference scheme just as in the steady state solution process. The same finite difference equations are used as in the steady state solution, equations 3.36 to 3.41. In this dynamic case, however, the time terms do matter so the m index is no longer disregarded.

47

The strain, aerodynamic force, and gravitational force are calculated once again for each cable segment and the endbody. These values are used to find the acceleration of each cable segment as well as endbody using their respective equations of motion. The main difference between the steady state and dynamic solution process is the added effect of aircraft motion. This factors in the solution process by affecting the placement as well as strain on the top end of the cable, while also altering the relative wind each segment is encountering. Once the acceleration of each position along the cable is solved for, the derivative state vector can be assembled. The ode45 solver than integrates these derivatives over a self-determined time step to arrive at the next point in time. The next point in time's state vector is then used to calculate the derivatives and the process repeats over the proscribed time span.

It is important to note, a requirement for the numerical solution to converge [3] [13] comes from the ratio of the time and spatial step, also known as the Courant number, $\delta \underline{t}/\delta \underline{s}$. For non-damping cable models, such as a Hooke's Law model which we are applying, the Courant number must be less than or equal to one [13].

3.6   Wake

The addition of wake effects on the cable and endbody is a relatively new foray into the study of cable towed decoy systems. Wake is generally more of an issue for low, slow, and heavy aircraft, such as cargo planes that have just lifted off or passenger planes that are on approach to land. However, during maneuvers, even lighter and faster tactical aircraft can create wakes that may affect the performance of a cable towed endbody. As the load factor of an aircraft increases, the circulation increases which leads to higher induced wake velocities. This becomes more apparent in the following theory. We first make a simplifying assumption, that the wake generated by the entire wing is characterized by two trailing wake vortices at the wingtips. This assumption allows the calculation of the wake effects in a timely manner, and is often used in research when estimating wake.

3.6.1 Wake Strength

The strength of the wake is dependent on a multitude of factors including aircraft weight, load factor, air density, airspeed, and planform area. Developed from Prandtl's lifting line theory, the Kutta-Joukowski theorem can be used to calculate the lift produced by a wing area. It is based on air density, airspeed, and circulation. In general, the theorem states that the lift, $\mathbf{L}$, produced by an element of a wingspan at position y along the span can be calculated by,

$$\mathbf{L}(y) = \rho_\infty \mathbf{U}_\infty \Gamma(y) \qquad , \qquad (3.42)$$

where $\mathbf{U}_\infty$ is the relative airspeed, ρ_∞ is the air density and $\Gamma(y)$ is the circulation[1]. Integrating over a wing, and assuming the lift distribution to be elliptical allows us to rearrange the theorem to solve for the circulation,

$$\Gamma_0 = \frac{4nW}{\pi \rho_\infty \mathbf{U}_\infty b} \qquad , \qquad (3.43)$$

$$\Gamma(y) = \Gamma_0 \sqrt{1 - (\frac{y}{b})^2} \qquad (3.44)$$

where b is the wingspan, n is the load factor and W is the weight of the aircraft. The circulation is key in finding the actual velocity induced by a wake vortex at any point in space. The planform area, weight, and air density are all givens in the solver, and the load factor and airspeed are found using the outputs of the aircraft simulation. This gives us all of the values needed to calculate the wake velocity induced on any segment of the cable or decoy.

3.6.2 Wake Induced Velocity

The velocity induced by the twin trailing wake vortices of an aircraft's wing span is found using the Biot-Savart Law. This law states that the velocity induced by a wake

49

vortex is a function of distance and wake strength. The law is given by,

$$\mathbf{dV} = \frac{\Gamma(\mathbf{dl} \times \mathbf{r})}{4\pi|\mathbf{r}|^3} \qquad , \tag{3.45}$$

where $\mathbf{dl}$ is the incremental length along the vortex filament and $\mathbf{r}$ is the vector distance between the vortex and the place in space where the velocity is induced[10]. In order to find the velocity induced by one of the trailing wake vortices, referring to figure 3-3, equation 3.45 can be re-arranged assuming the wake strength, Γ remains constant,

$$\mathbf{V} = \frac{\Gamma}{4\pi r_p} \int_{\theta_1}^{\theta_2} sin\theta d\theta \qquad , \tag{3.46}$$

$$V = \frac{\Gamma}{4\pi r_p}(cos\theta_1 - cos\theta_2) \qquad . \tag{3.47}$$

A separate function is created in Matlab to integrate the effects of all segments of the trailing wake on each piece of the cable system at each timestep. Because the wake is segmented, it is assumed that the wake strength remains constant only in each segment, allowing the use of the equations. The trailing wake is segmented into enough pieces, $.05s$ timestep, where this assumption should be valid. The function returns the velocities received by the decoy system program where they are added to the velocity and apparent wind that each segment of the cable and endbody encounters during the maneuver. Because the process is repeated for each timestep, and the integrations are time and memory consuming, a mex file is used to bridge between Matlab and the more loop friendly C++ where the actual wake function is written.

The basics of the wake field calculation come from equation 3.46. The wake field function segments a trailing wake filament into particular lengths in order to calculate the velocity induced at a point on the cable by the integration of those segments. It is then added to the velocity induced by the second wake filament. This process is looped for every segment of the cable as well as the endbody.
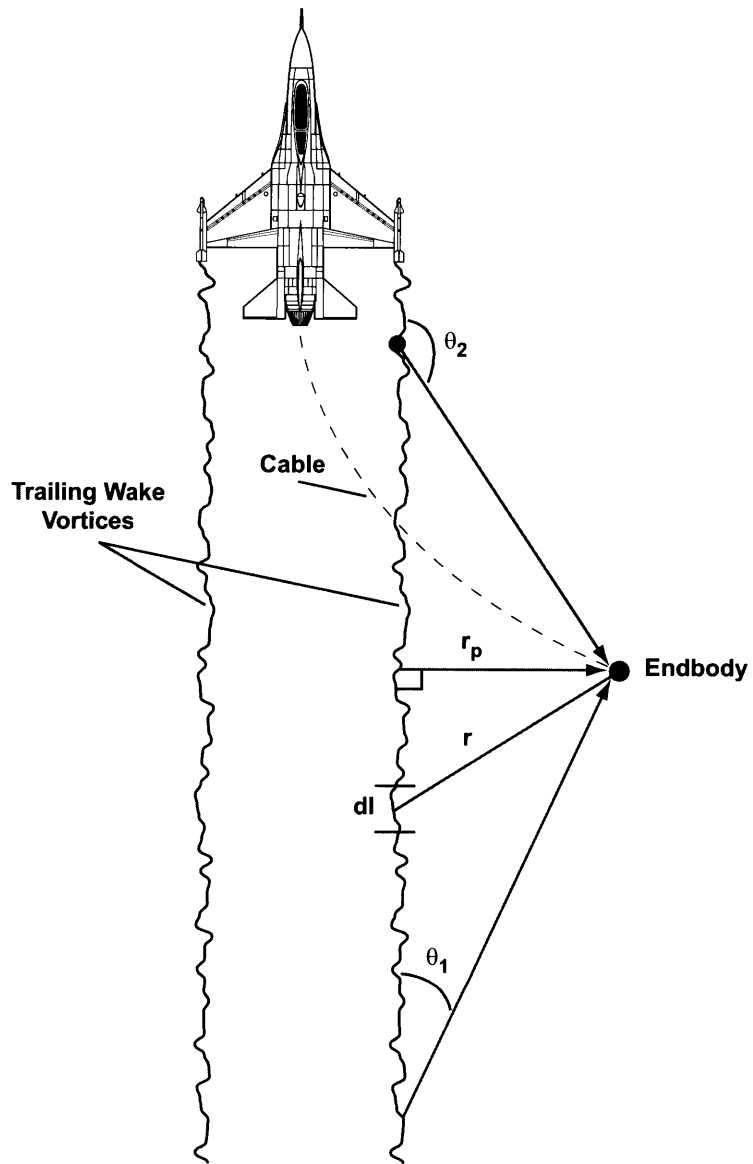
Figure 3-3: Calculating Wake Velocity

Chapter 4

Comparison to Other Models

As was shown in the previous literature review, many researchers have developed tools to analyze cable-towed endbodies in various manners. In order to assess the accuracy of the model created herein, a few of the other models were analyzed. Three completely different models are shown to match up very well with the model created in this thesis. The graphical results of the other author's models were first scanned and then digitized using a code written in Matlab.

Two of the models are chosen for their relatively recent publication, and the third is chosen to compare the model during its dynamic state. Unfortunately, the wake effects are not compared. Only one other paper [27] has used wake effects but they did not report or analyze the cable shape or endbody position when subjected to wake. Therefore, the wake effects created by the model presented here are nullified in order to accurately compare across models.

4.1   Zhu and Meguid

Zhu and Meguid have focused the majority of their research in the area of aerial refueling modeling[27][26]. From a modeling point of view, the major differences between an aerial refueling hose and a cable are the length, the material properties, and the diameter. Their model included a refueling hose and a drogue apparatus, these are modeled using the cable and endbody respectively. Zhu and Meguid's steady

Table 4.1: Zhu and Meguid Critical Parameters

Parameter	Value
Air Density ρ	$1.22 \ kg/m^3$
Airspeed	$131 \ m/s$
Hose (Cable) Length	$23.77 \ m$
Hose (Cable) Outside Diameter	$0.0673 \ m$
Hose (Cable) Elastic Modulus	$336 \ MPa$
Hose (Cable) Linear Density	$2.39 \ kg/m$
Hose (Cable) Normal Drag Coefficient	1.18
Hose (Cable) Tangential Drag Coefficient	0.02
Drogue (Endbody) Mass	$29.5 \ kg$
Drogue (Endbody) Drag	$0.232*$(dynamic air pressure) N

state shape was evaluated with the aircraft traveling at $255 \ KTAS$ or $131 \ m/s$. The important parameters are found in Table 4.1, which were followed exactly in order to compare to the work done by Zhu and Meguid. The two steady state shapes are plotted against each other in Figure 4-1. In the figure, the origin is located at the top right, where the cable is connected to an aircraft traveling from left to right. The endbody is located at the bottom left end of the cable floating in the freestream.
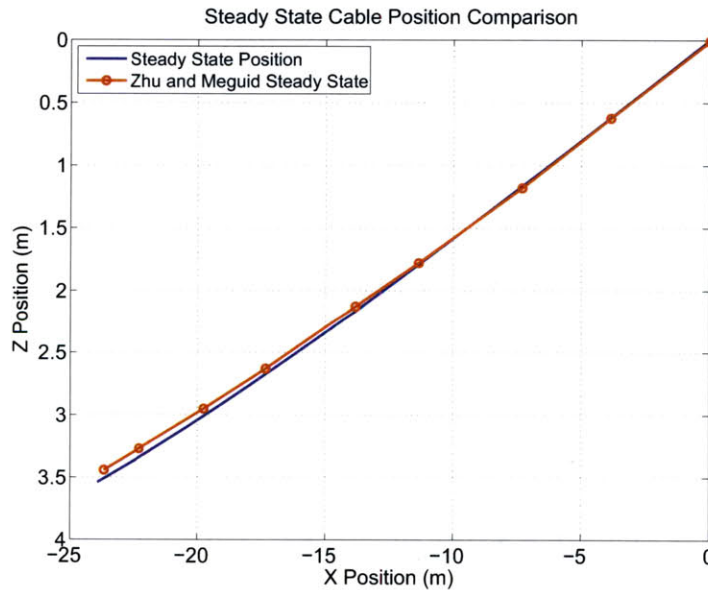
Figure 4-1: Steady State Comparison to Zhu and Meguid, 29.5 kg Drag sphere, $C_d = 0.5$, $U_0 = 131 \ m/s$ on 23.77 m extensible Cable
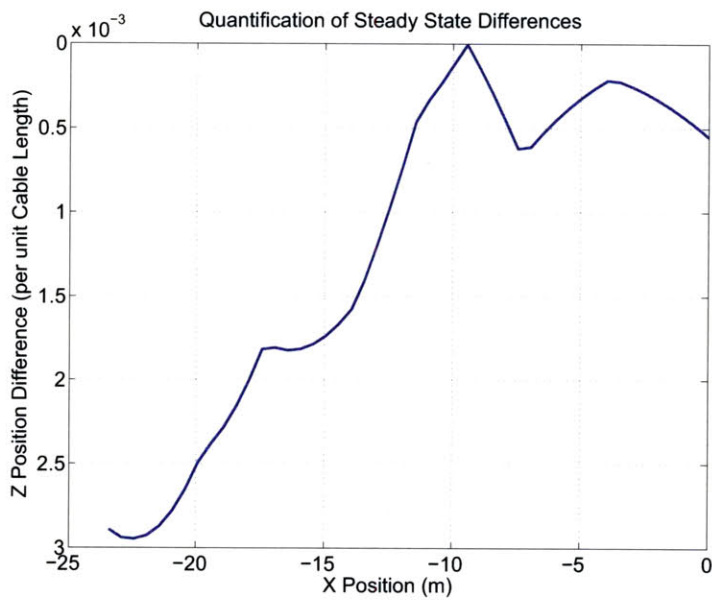
Figure 4-2: Quantification of Steady State Differences between Zhu and Meguids and Thesis Model, 29.5 kg Drag sphere, $C_d = 0.5$, $U_0 = 131$ m/s on 23.77 m extensible Cable

Figure 4-2 shows the quantity of the difference between the two models. As you can see, the maximum difference occurs at the endbody end of the cable, for a total difference in placement of 0.3%. A possible source of difference arises from the modeling methods. Zhu and Meguid's model uses a finite element method with a three-noded curved beam element. This method differs from the finite difference method used in this thesis because it can be used with more complex geometries which have properties that vary along the cable, whereas the finite difference method is usually quicker to implement and less computationally demanding. It was also necessary to alter the manner in which drag was being calculated in order to perfectly align the two processes, as Zhu and Meguid calculated the normal and tangential drag coefficient's using different constants while still using the cross-flow principle. They also calculated bending and torsional moments on the cable within their modeling process, neither of which are calculated in this thesis.

As you can see in Figure 4-1, the two models predict very similar behavior at a steady state configuration even with the aforementioned differences in modeling techniques. The steady state cable appears slightly different, most likely due to their assumption the hose tension was equal to the drag of the drogue, whereas the tension calculated in the steady state depends on the drag and lift of the endbody as well as the entire cable. Because of the slight difference, however, it was necessary to compare the steady state model to another recently published thesis.

4.2 Hill and Richardson

Hill and Richardson both studied and researched the dynamics of towed cable decoys in the years of 2005 and 2006 at the Air Force Institute of Technology (AFIT). As was described, their research focus was on the thermodynamic aspect of towed decoys crossing into the jet plume of a combat aircraft[3][4]. Richardson conducted multiple parametric studies on towline shape, while Hill incorporated that modeling into a dynamic environment and studied the effects encountered from the extremely hot exhaust gases behind the aircraft.

Table 4.2: Hill and Richardson Critical Parameters

Parameter	Value
Air Density ρ	0.55 kg/m^3
Airspeed	50 m/s
Cable Length	30 m
Cable Diameter	0.00127 m
Cable Elastic Modulus	200 GPa
Cable Density per Length	0.0096 kg/m
Cable Normal Drag Coefficient	1.1
Cable Tangential Drag Coefficient	.04
Endbody Mass	1 kg
Endbody Drag Coefficient	1

Both authors used roughly the same model and their steady state's were nearly identical as shown in Hill's Figure 4.2-1[3]. The main difference between this model and the AFIT student's model is their assumption that the cable is inextensible. This is a potential source of error in comparison, however, the cable properties shown in Table 4.2 minimize this source as the endbody is relatively light, has normal drag, and the cable is relatively short, therefore minimizing the impact of an extensible cable. This steady state, and its associated parameters were given to the cable model presented herein and the comparison is shown in Figure 4-3. The figure, as will be standard, depicts the aircraft transitioning from left to right across the page with its tow cable attachment point at the origin of the coordinate system at the top right, with the endbody hanging freely at the bottom left end of the cable.
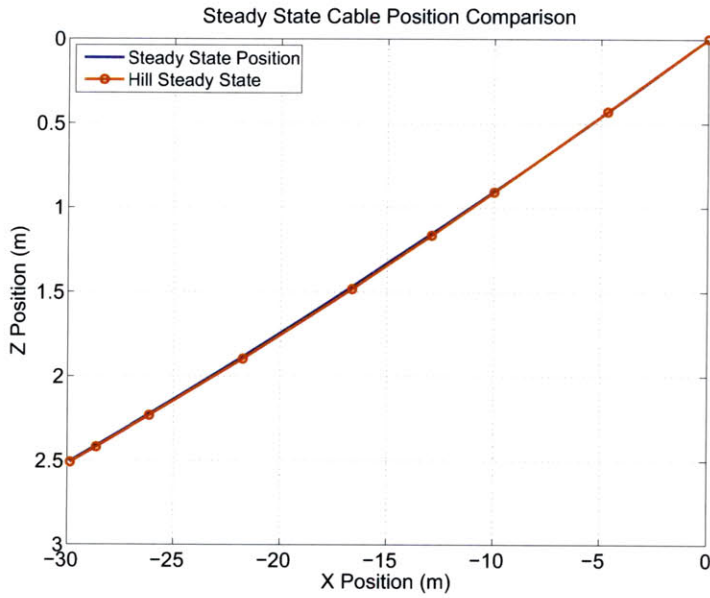
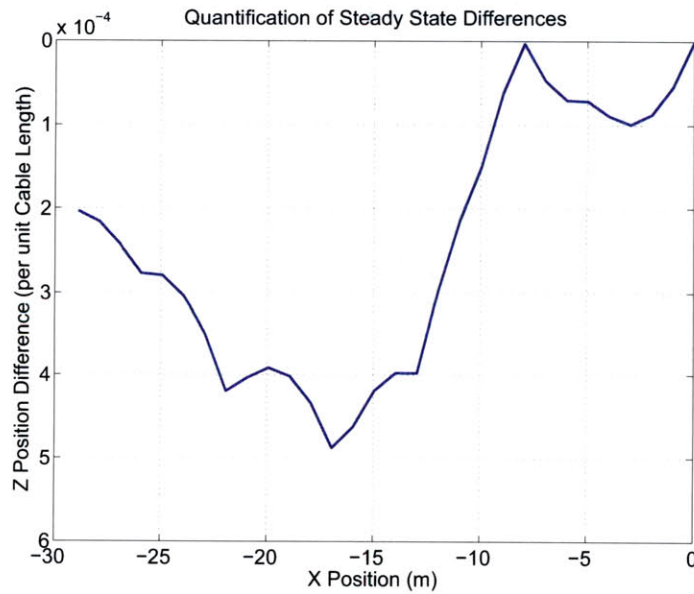Figure 4-3: Steady State Comparison to Hill, 1kg Drag sphere, $C_d = 1$, $U_0 = 50\ m/s$ on $30\ m$ inextensible Cable

Figure 4-4: Quantification of Steady State Differences between Hill and Model, 1kg Drag sphere, $C_d = 1$, $U_0 = 50\ m/s$ on $30\ m$ inextensible Cable

Figure 4-3 shows the two models predicting the same steady state position for the given conditions, or as close as can be expected for a digitized plot. Note the difference in C_d and U_0 from the previous comparison. Figure 4-4 shows the quantity of the difference, in per unit cable length values, along the length of the cable during the steady state. As it shows, the maximum difference is 0.05% which occurs surprisingly near the midpoint of the cable. This error, because it is so minor, could have been caused by the actual digitization process, as points along the plot are picked by mouse and translated into Matlab coordinates for comparison. Both comparisons so far have remained steady and had similar cable lengths. The third comparison deals with both of these issues, as a dynamic comparison is presented at extremely long towline lengths.

4.3 Karlsen

Karlsen and a team of Swedish researchers contributed to the study of aerially towed endbodies by subjecting them to small maneuvers while assuming the cable was in-extensible. The endbody drag and weight was varied across a few different runs, as well as the towline length. The table below highlights the main parameters used in these runs used for comparison. It is important to note that Karlsen assumed an inextensible towline, mainly to save computation time, and differences are to be expected between the two models because the towline length and endbody parameters produce a favorable environment for cable lengthening.

The values in Table 4.3 highlight a portion of the parameter range the Swedish researchers were interested in. The length of the towline is the main difference, as it was varied between values of 2 km and 5 km. The research team analyzed the cable system in a few simple maneuvers, and their results were presented by means of endbody height, tension, and cable shape. Multiple plots from Karlsen's report[12] were digitized and then compared to the results given by the presented model.

The maneuver most common in their results is a simple turn maneuver. In this action, the aircraft is completing a 180 degree turn in the time span of 50 s with

59

Table 4.3: Karlsen Critical Parameters

Parameter	Value1	Value2
Air Density ρ	$1\ kg/m^3$	-
Airspeed	$150\ m/s$	
Cable Length	$2000\ m$	$5000\ m$
Cable Diameter	$0.002\ m$	-
Cable Elastic Modulus	$200\ GPa$	-
Cable Density per Length	$0.02\ kg/m$	-
Cable Normal Drag Coefficient	1.15	-
Cable Tangential Drag Coefficient	.015	-
Endbody Mass	$5\ kg$	$25\ kg$
Endbody Drag Coefficient	0.75	0.25

an approximate bank angle of 45 degrees. The aircraft begins the turn at time zero and pulls out of the turn at the 50 s mark. 100 s of results were provided in the report, to show the differences between steady state and turning cables. Figures 4-5 and 4-6 show the comparison with a relatively light endbody with normal drag characteristics that is being towed by a 2 km cable through the simple turn maneuver. The results of this model align with the results given by Karlsen with a slight offset. Small differences are observed in the endbody position below the aircraft, roughly 5 m at some points, which can be expected considering the extreme towline length, the extensibility difference, and the maneuvering aspect of the model. The tension reported at the aircraft is also slightly different, which can be attributed to the inextensible assumption as well. Figure 4-6 also shows a slight dip in the reported tension at the aircraft, which is not replicated by this model. This dip is most likely due to the inextensible assumption, as the aircraft is nearing the end of the turn at the 50 s mark, and the cable maybe swinging too far past the aircraft in the lateral direction.
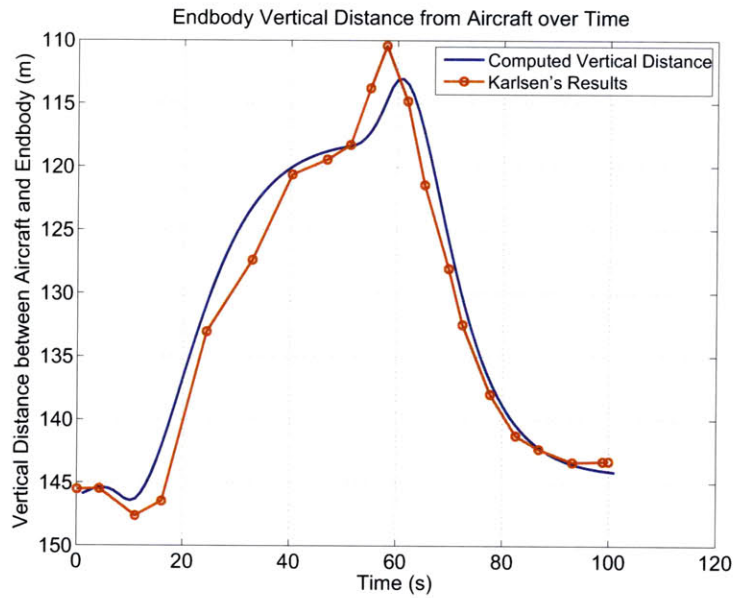
Figure 4-5: Endbody Distance from Aircraft During Turn, 5kg Drag sphere, $C_d = .75$, $U_0 = 150\ m/s$ on $2000\ m$ inextensible Cable
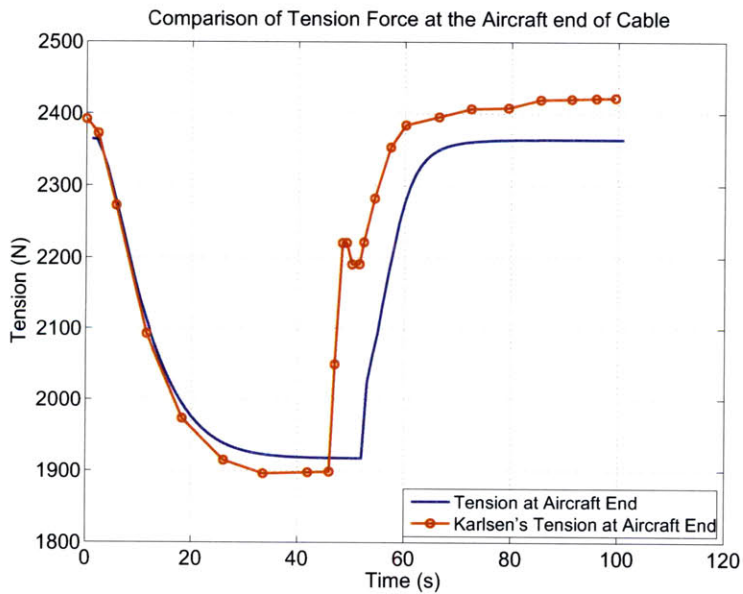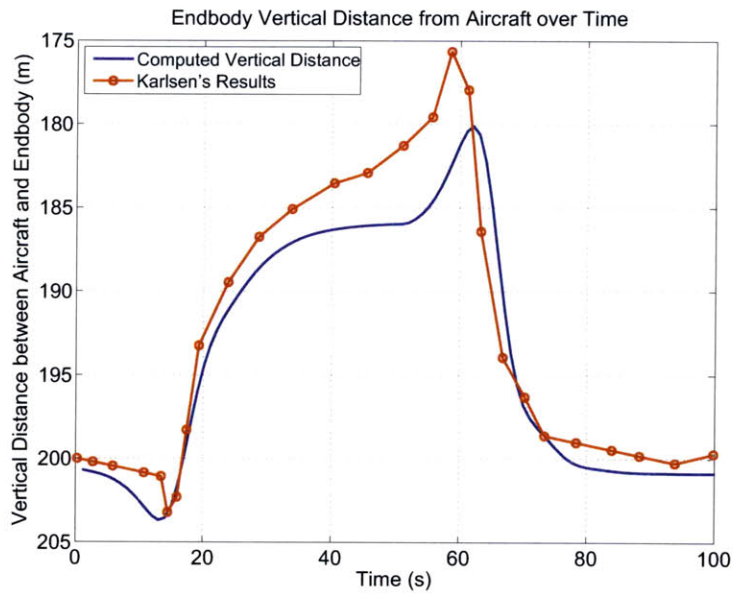

Figure 4-6: Cable Tension at the Aircraft During Turn, 5kg Drag sphere, $C_d = .75$, $U_0 = 150\ m/s$ on $2000\ m$ inextensible Cable

With a heavier endbody exhibiting less drag, the results are also not exactly the same. Figure 4-7 shows that once the dynamic portion of the maneuver occurs, the models predict the same behavior, however, the endbody is slightly lower than predicted by Karlsen. This is caused, most likely, by the inextensible assumption, as the cable is going to stretch some due to the higher mass of the endbody, 25 kg in this run as compared to the previous comparison. Figure 4-8 shows the cable tension at the aircraft, which also differs due to the inextensible assumption by Karlsen. The slight differences can also be attributed to the fact that the spatial step chosen by Karlsen is very large. He specifies only 100 segments along the cable, therefore the spatial step for the 2 km cable is 20 m. Small differences are expected, as each model tries to solve the system it can only be so accurate due to the large segment sizes. Any difference in the solution process would be magnified by the time the solver finds the endbody position due to the extremely long cable length. A perfect match seems quite unreasonable for a maneuvering cable system under these circumstances. Also, a small amount of error can be attributed to the digitization process, which relies on a user's ability to accurately trace the author's figure using a computer mouse.

Figure 4-7: Endbody Distance from Aircraft During Turn, 25kg Drag sphere, $C_d = .25$, $U_0 = 150 \ m/s$ on 2000 m inextensible Cable
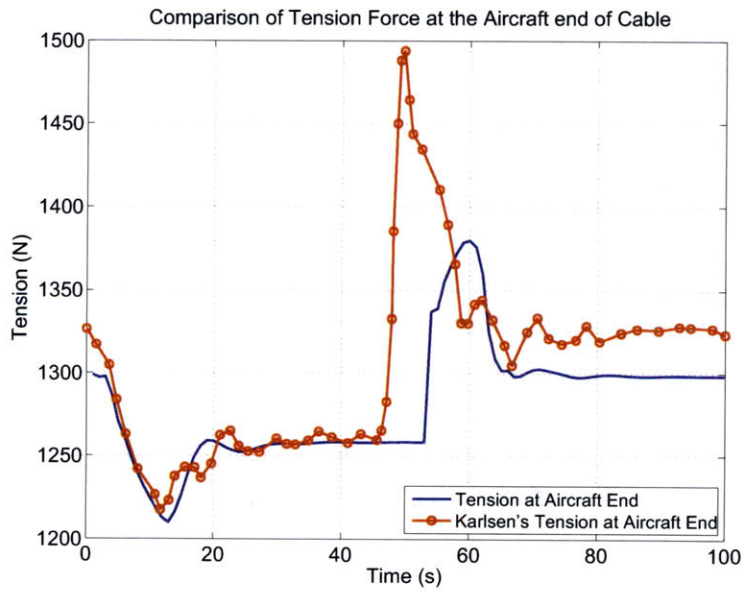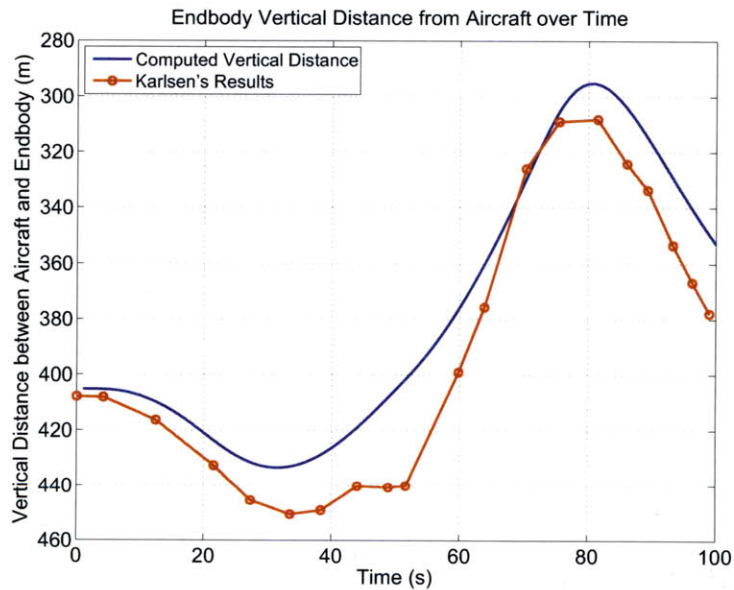

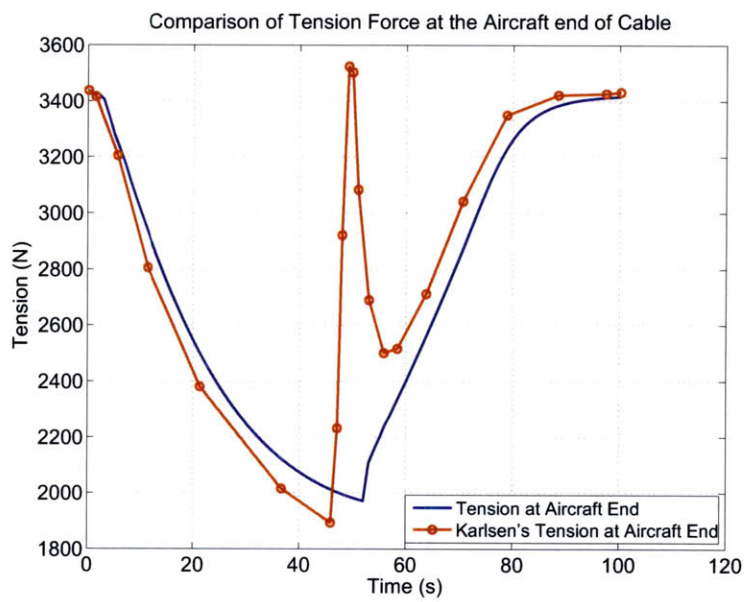Figure 4-8: Cable Tension at the Aircraft During Turn, 25kg Drag sphere, $C_d = .25$, $U_0 = 150 \ m/s$ on 2000 m inextensible Cable

63

Finally, a longer towline of 5 km is analyzed. As you can see, in Figure 4-9, the endbody position below the aircraft is actually predicted to be higher than the position predicted by Karlsen. Once again, the small differences could be due to the large step size of 50 m. The predicted endbody positions are on average 25 m apart and for a towline of 5 km this seems like a close comparison. As you can see, the endbody does not completely return to the steady state level as the maneuvering time is completed because of the extremely long cable length. It would take longer than 100 s to return to initial conditions. The tension at the aircraft is also very close as seen in Figure 4-10 besides the spike at around 50 s that appears in Karlsen's model. This spike may have been caused by their inextensible assumption because at that time the aircraft is finished turning and the cable and endbody system is swinging through the end of the turn and its rotational inertia is changing directions.

Figure 4-9: Endbody Distance from Aircraft During Turn, 5kg Drag sphere, $C_d = .75$, $U_0 = 150$ m/s on 5000 m inextensible Cable

Figure 4-10: Cable Tension at the Aircraft During Turn, 5kg Drag sphere, $C_d = .75$, $U_0 = 150 \ m/s$ on $5000 \ m$ inextensible Cable

Chapter 5

Results and Analysis

5.1 Parameters and Set-Up

For the maneuver and wake effect analysis that follows, a set of common cable and endbody parameters are employed, found in Table 5.1. Most of the values are chosen to closely resemble previous researchers parameters, while some are added and estimated in order to provide values for the wake calculation, such as an aircraft planform area and mass. Steel and Kevlar cable properties are used, along with a simple drag sphere as the endbody.

The cable endbody system, with the parameters noted, was maneuvered through three types of flight. First, like the comparisons in Chapter 4, involves the aircraft flying straight with a constant altitude. The second maneuver is a basic, 180 degree turn by the aircraft at a constant altitude. The turn is conducted at varying levels of load factor as well as varying cable length and material. The aircraft flies straight for a portion of time depending on the length of the cable, then banks into a left turn, where the bank angle increases rapidly to reach and maintain the angle needed to reach a specified load factor. Once the heading has changed 180 degrees, the aircraft rolls out of the bank rapidly back to level flight. Because the aircraft is treated as a general tactical aircraft, and most modern tactical aircraft can achieve very high instantaneous roll rates, the steady bank angle is reached within one second. The third maneuver is a climb, where the aircraft pitches up to gain altitude until leveling

Table 5.1: Cable and Endbody Standard Parameters

Parameter	Value
Reference Altitude	4000 m
Air Density ρ	.819 kg/m^3
Airspeed	200 m/s
Cable Length	25 - 1000 m
Cable Diameter	0.002 m
Cable Material	Kevlar and Steel
Cable Elastic Modulus	62 and 200 GPa
Cable Density	1400 and 7600 kg/m^3
Cable Normal Drag Coefficient	1
Cable Tangential Drag Coefficient	0.1
Endbody Mass	10 kg
Endbody Drag Coefficient	1.2
Aircraft Wing Span	10 m
Aircraft Planform Area	25 m^2
Aircraft Mass	9000 kg

off at a specified altitude. The pitch angle is dependent on the amount of altitude to climb, as each maneuver is conducted in the same timespan of 45 s. The climb is conducted with varying levels of altitude gain, as well as cable length and material. These basic maneuvers provide a starting point for analysis of the cable endbody system which can be easily modified for future research. In each case, results are compared with and without the trailing wake.

5.2 Wake

5.2.1 Wake Segment Spacing

To accurately model the effects of the wake velocity induced on each part of the cable and endbody, the two trailing wake vortices must be segmented into pieces and then integrated across the whole length. The size of the pieces, which depend on the wake function's timestep, greatly impacts the processing time. The smaller the wake function's timestep, the longer the process takes, and for large maneuvers, it can take hours to finish a single maneuver with a minimal timestep. However, a time step that is too large does not accurately represent the maneuver, especially if the wake

filaments are twisting and turning.

In order to find a balance between time and accuracy, the straight and level maneuver and the 180 degree turn maneuver are conducted with varying wake timesteps. The results appear in Figures 5-1 and 5-2. These figures show the maximum wake induced velocity felt along the cable at each timestep. In the straight and level flight the results seem to converge at a timestep of .1 s, however the turn maneuver figure shows the wake velocity function converges at a timestep of .05 s.

Maximum Wake Induced Velocity Along Cable
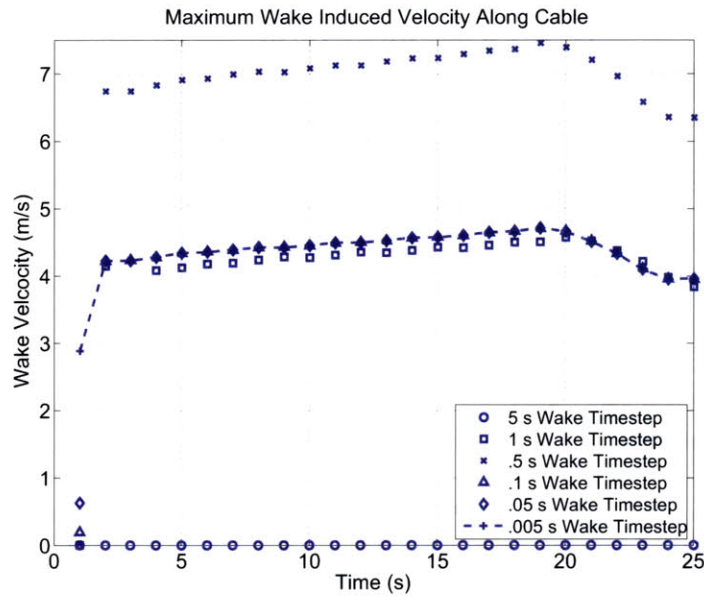
Figure 5-1: Effects of Wake Spacing on Maximum Wake Induced Velocity during Straight and Level Flight, 50 m Steel Cable
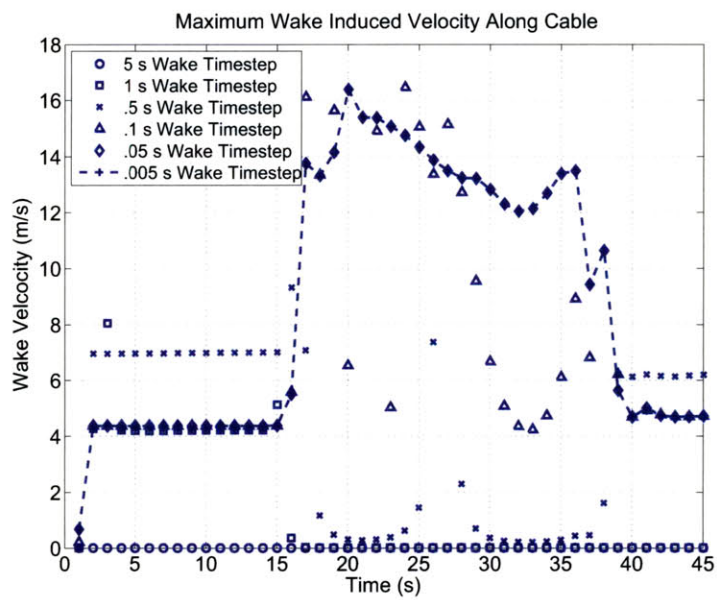
Figure 5-2: Effects of Wake Spacing on Maximum Wake Induced Velocity during 180 Degree, 3-g Turn, 50 m Steel Cable

In order to be completely accurate, the cable shapes as well as endbody positions are also examined with the various wake timesteps. Figure 5-3 shows how a 0.05 s wake time step is accurate for the straight and level flight. This figure details the distance below the aircraft which the endbody is vertically displaced. This type of plot is the same in which Karlsen detailed endbody motion during his turn maneuvers, and is used frequently in the thesis to detail endbody movement during maneuvers. It shows the timestep of .1 s not completely converging with the .005 s timestep result. The .05 s timestep example, however, does converge for this selected cable length. Figure 5-4 shows that the cable shape also differs between the selected wake time steps, with .1 s being the largest time step that still provides for a cable difference due to wake velocity, however, the .05 s timestep is slightly more accurate.
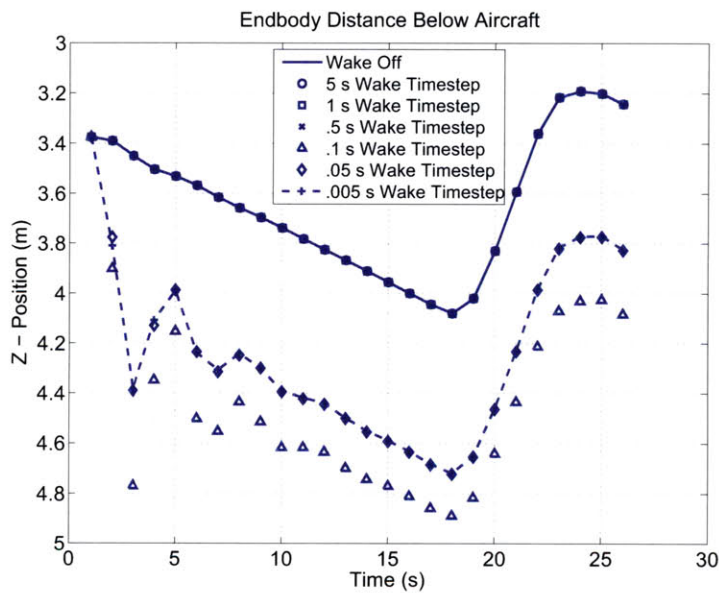
Figure 5-3: Endbody Distance Below Towing Aircraft Dependence on Wake Function Timestep During Steady Flight for 50 m Steel Cable
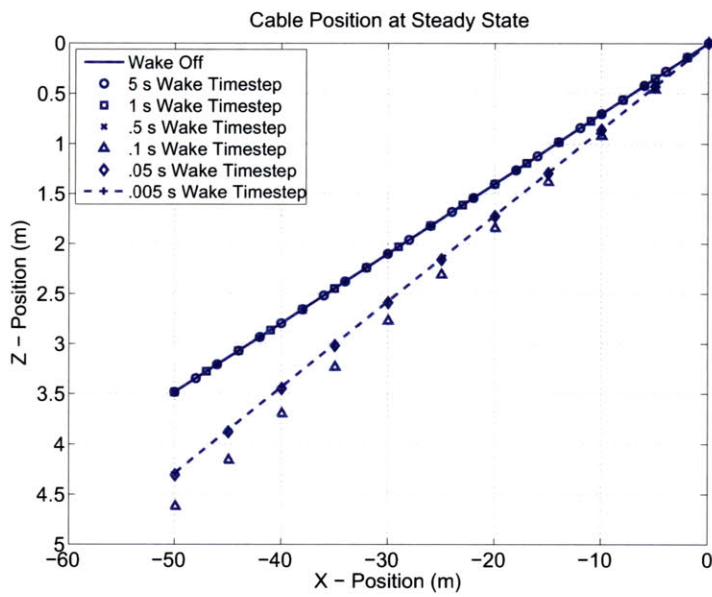
Figure 5-4: Cable Shape Dependence on Wake Function Timestep During Steady Flight for $50\ m$ Steel Cable

This investigation was repeated for the turn maneuver, which could require an even smaller timestep as the wake is changing directions and orientations while the aircraft is maneuvering through the turn. The results are shown in Figure 5-5. It shows that the timesteps of $.05\,s$, and $.005\,s$ coincide while the $.5\,s$ timestep falls inline with the wake-less example and the $.1\ s$ timestep is only inaccurate throughout the turn, something that must be avoided. In order to be completely accurate, a wake time step of $0.05\ s$ is used for all cases in which a $50\ m$ cable is used. It is found that the wake timestep can be increased to $.1\ s$ for larger cables and remain just as accurate.
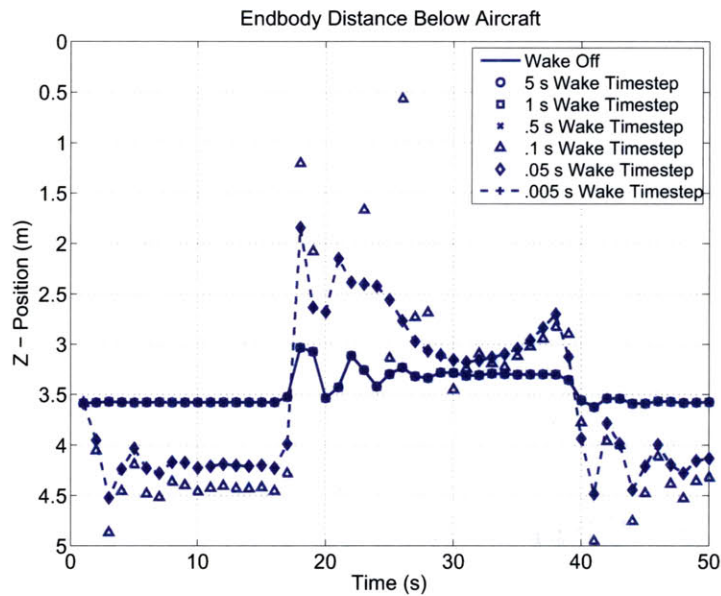
Figure 5-5: Endbody Distance Below Towing Aircraft Dependence on Wake Function Timestep During Turn Maneuver for $50\ m$ Steel Cable

5.2.2 Wake Activity Distance

Another issue that appears in the wake calculation is the length in which a segment of the trailing wake vortex is affecting the cable and endbody system. For an aircraft traveling straight and level, the segment of wake created $2km$ prior will only negligibly affect the cable and endbody system. Due to computational requirements of the Matlab function that is calculating the wake induced velocity on the system, it is necessary to disregard segments of the trailing wake that are minimally affecting the cable system. The distance for which a released segment of the wake is contributing to the wake velocity induced along the cable is referred to as the wake activity distance.

The cable model was run through a short, level flight maneuver while using two different wake activity distances. The aircraft was traveling at $200\,m/s$, so 5 seconds of activity would give $1\,km$ of active wake segments as opposed to 2 seconds giving $400\,m$ of wake activity. Because this may be more of an issue for longer cables, where a longer active wake portion would be closer to the longer length of the cable, the cable length investigated is $1\,km$.

Figure 5-6 shows minute differences between a $400\,m$ and $1\,km$ activity distance on the level flight maneuver. The lack of effect by the increased wake activity distance is most likely due to the longer cable lines being less affected by the wake to begin with. Their increased mass, when compared to a shorter length, allows the cables to absorb more wake induced velocity and dampen it throughout the cable. It may also be due to vertical distance between the wake and cable, which becomes larger the further away from the aircraft you are, therefore the wake is inducing less velocity at the farthest points of the cable.

In order to completely catalog the results, the same negligible effect of extra wake activity distance is appears for both turn and climb maneuvers as well. The turn results are seen in Figure 5-7. The climb maneuver produced the same negligible difference and is not presented. Because of the lack of effects and the importance of computational resources a wake activity distance of $400\,m$ is used for all of the runs following.
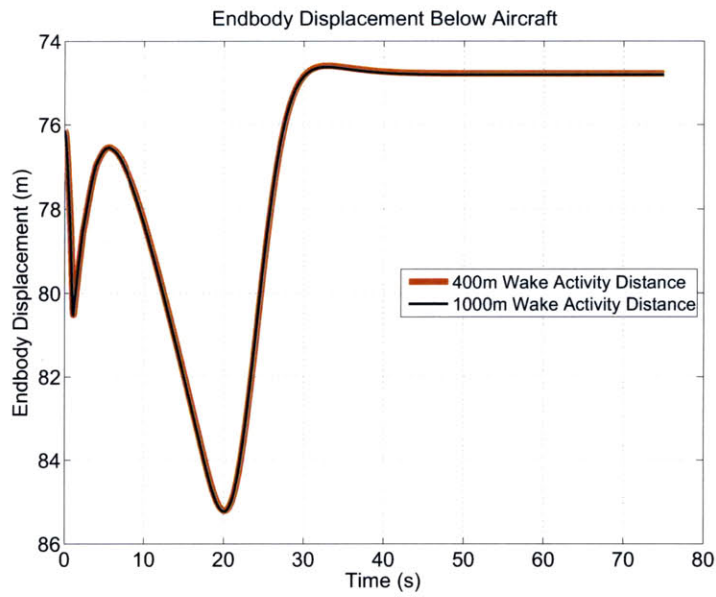
Figure 5-6: Comparison of Endbody Distance below Aircraft During Maneuver for $400\,m$ and $1000\,m$ Active Wake Distance with $1\,km$ Steel Cable
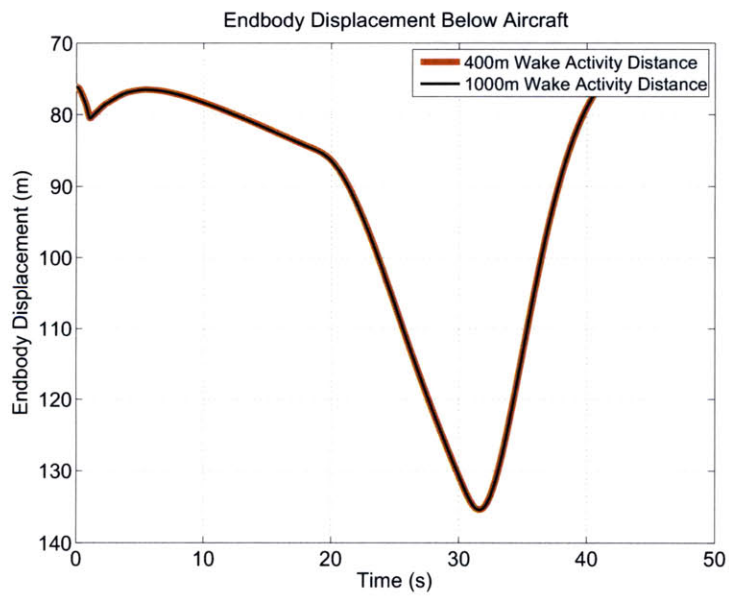

Figure 5-7: Comparison of Endbody Distance below Aircraft During Turn Maneuver for $400\,m$ and $1000\,m$ Active Wake Distance with $1\,km$ Cable

5.2.3 Steady Level Flight

Now that the assumptions have been explained, the actual effects caused by adding a wake field to the cable endbody system are examined. In steady, level flight, Figure 5-8 shows the difference in cable shapes between a wakeless and wake induced example. The induced velocity clearly pushes the entire cable system in the positive Z direction, towards earth, along most of the cable. The effects appear to travel down the length of the cable and impact the endbody position the most. This is seen in Figure 5-9, which shows how much of the displacement is caused by the wake at three points along a 50 m steel cable. The initial perturbation is due to the onset of the wake which is not pre-calculated for the steady state position. The endbody is displaced about 0.6 m below the results from a wake-less example. This effect seems trivial but during steady, level flight a light tactical aircraft is producing minimal wake and this is to be expected.
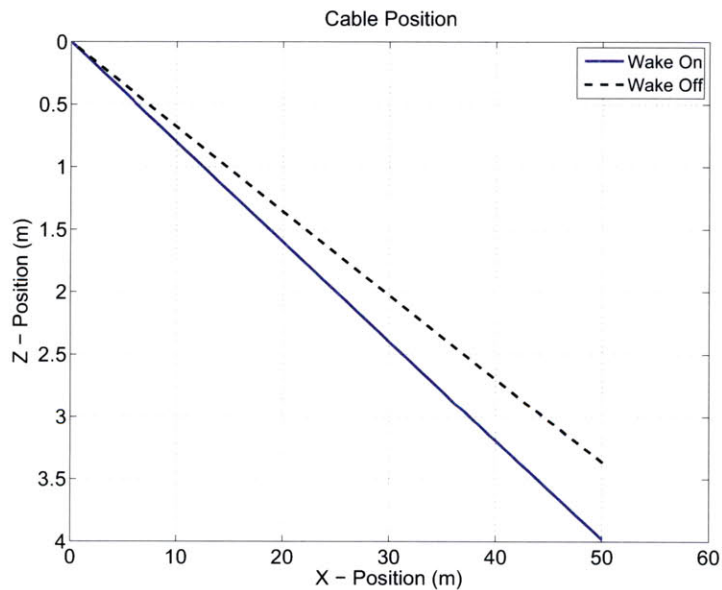
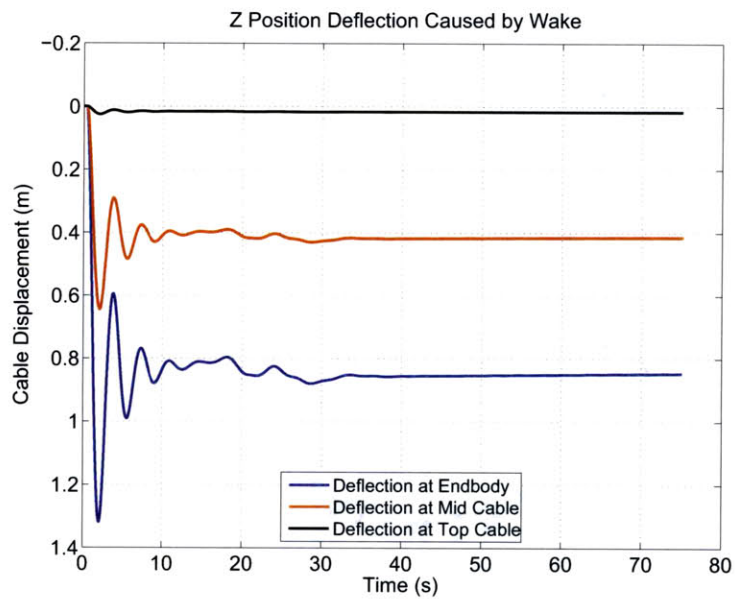Figure 5-8: Steady State Cable Shape with or without Wake, 50 m Steel Cable

Figure 5-9: Cable Displacement Due to Wake, 50 m Steel Cable

The straight and level flight case is repeated with greater cable lengths which show that the wake is still affecting the cable shape at the 300 m length, by pushing the cable down half of a meter, however, at lengths greater the effects become minimal. It is also repeated with a different cable material, Kevlar. A cable comprised of Kevlar 29, a proprietary material made by DuPont, has a density of 1440 kg/m^3 and an elastic modulus of 62 GPa[15][23] with tensile strength of 400 GPa. This material provides the same strength as steel at about 20 percent of the weight[23].

As the results show, both materials are minimally affected by the wake in Figure 5-10. This figure shows the Z-position deflection of the endbody at various lengths due to the wake effects, or the difference between the endbody position with and without wake. The deflection is normalized by the length of the cable. As is shown, the max deflection for steel is about 1.7% which occurs at the 25 m cable length, with similar results for Kevlar.

The highest percentage deflection occurs around 25 m where nearly 0.5 m of displacement occurs. The endbody deflection caused by the wake is minimal at longer lengths, such as the 500 m and 1 km cables. They exhibit minimal deflection due to their larger mass and inertia which is affected less by the same amount of wake strength than the shorter, lower mass cables.

The similar, minimal deflections appear again in runs conducted with Kevlar towing cables. The main difference between the Kevlar and steel cables is shown in the overall shape of the cable, as the Kevlar cable is minimally higher in position than the steel cable. This is because the mass difference in cable, as the steel cable has a higher density, therefore the gravitational force can counteract more of the drag force exhibited by the cable body system. This appears in Figure 5-11, which shows the relative shapes of a 50 m cable comprised of steel and Kevlar. The Kevlar cable is also extending more, by 0.5 m, due to its smaller modulus of elasticity than the steel cable.
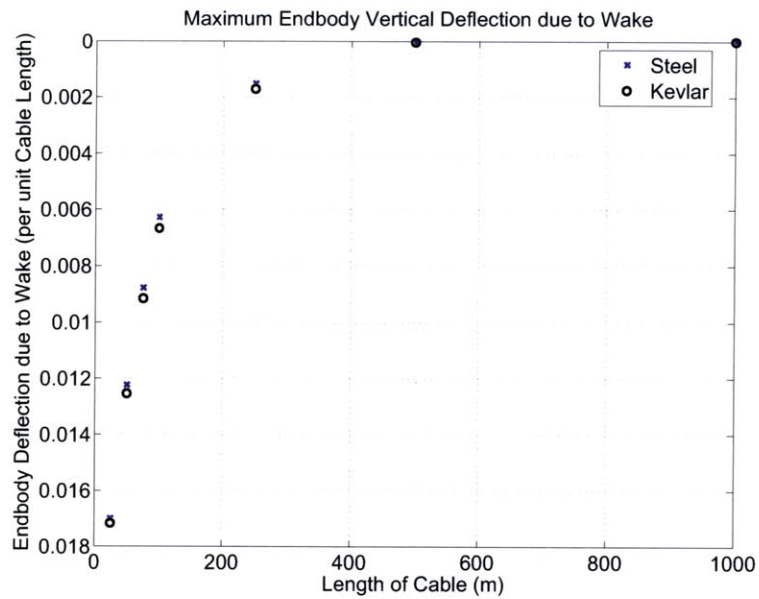
Figure 5-10: Endbody Deflection below Aircraft due to Wake Effects During Level Flight with Varying Lengths of Steel and Kevlar Cable
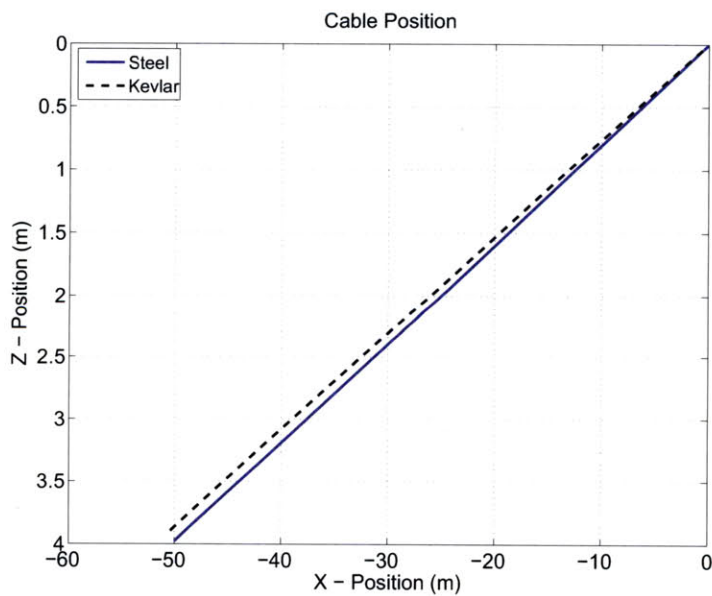

Figure 5-11: Comparison of Endbody Distance below Aircraft due to Wake Effects During Level Flight with $50\,m$ Kevlar and Steel Cables

5.3 Turn

The second maneuver analyzed is the turn maneuver. This maneuver is the same one that Karlsen[12] researched, where an aircraft is initially headed in one direction for a short period of time, $3 - 5\,km$ depending on the aircraft specified velocity, and then turns 180 degrees. The length of cable, material of the cable, as well as the aircraft's load factor were all varied to find the results following. The initial turn comparison is conducted using a simulated level turn in which the aircraft's load factor peaks at 4.5 after a steady ramp up with a steady ramp down following the apex of the turn.

The following, Figure 5-12, shows that the endbody deflection due to wake is minimal for long cable lengths. This figure shows the maximum endbody Z-position difference throughout an entire turn, between runs conducted with and without wake. The deflection is once again normalized by the length of the cable, as you can see the maximum displacement is about 3.2% which occurs with the $25\,m$ cable. The results are strikingly similar to the level flight case.

Overall, more displacement is occurring in the turn than level flight due to the increased load factor of the aircraft, as it affects the strength of the wake circulation as shown previously in equation 3.43. The results also show the Kevlar cables experiencing more overall deflection than steel cables. Although Kevlar cables are above steel cables during level flight as shown in Figure 5-11, they are affected more during turn maneuvers. This occurs because of their lower mass, as the additional strength in wake can affect its position to a greater extent. Therefore, the wake causes Kevlar to displace more, and thus appears more affected in the figure.
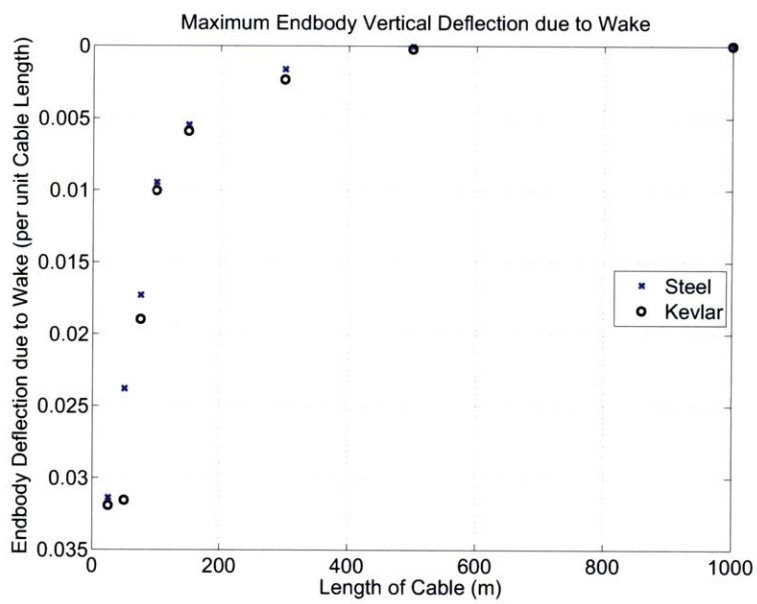
Figure 5-12: Maximum Endbody Deflection due to Wake Effects in the Z Direction During Level, 4.5-g Turn Maneuver with Varying Lengths of Steel and Kevlar Cable

Table 5.2: Turn Times

Load Factor	Start Time	End Time
3 g	15.0 s	37.6 s
5 g	15.0 s	28.1 s
7 g	15.0 s	24.3 s

Figure 5-13 shows the endbody deflection in the Z-plane due to wake during three different load factor turns. The increase in deflection during the first few seconds is due to the initial onset of the wake, as the steady state solver does not incorporate the wake function. Once the aircraft begins the turn, at 15 s, the varying load factors show interesting results. The 7-g turn displaces the endbody the most in the vertical direction at the onset of the turn, which is expected as it is producing the greatest amount of wake strength due to its highest load factor.

The wake actually causes the endbody to rise above the position of a wake-less endbody at certain times during the turn. This is due to a larger amplitude of oscillation that is caused by the increase in wake strength at the beginning of the turn. The wake-less example does not experience the sudden onset of increasing wake strength while the aircraft's load factor suddenly rises, therefore it does not react with as much force as an example with the wake incorporated. Figure 5-14 shows the difference in endbody oscillation amplitude for the same 7-g turn conducted with and without wake. The same results appear with the Kevlar cables, therefore, only the steel cables are presented.
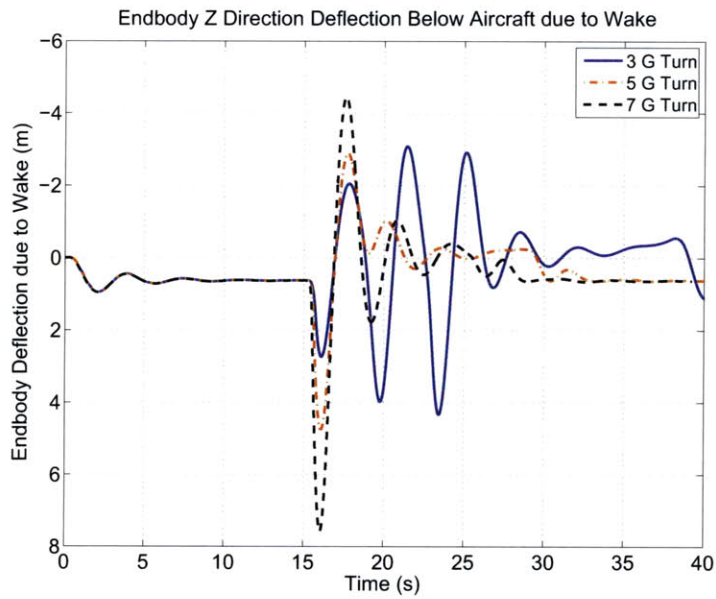
Figure 5-13: Endbody Deflection due to Wake Effects in the Z Direction During Varying Load Factor Turns with 50 m Steel Cable
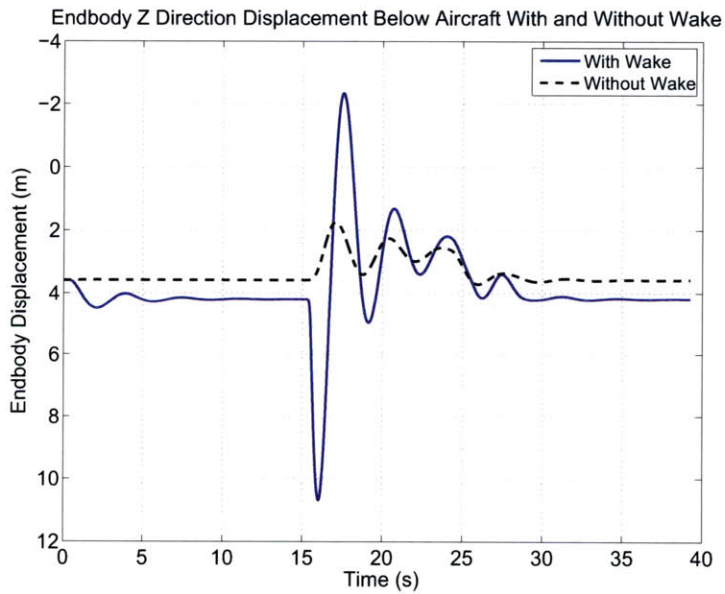

Figure 5-14: Comparison Endbody Displacement in the Z Direction During 7-g Turn Maneuver with 50 m Steel Cable, With and Without Wake

The wake effects were also examined in the lateral plane, or the positive Y direction which points out the right wing of the aircraft. The lateral displacement is the difference between the cable position in the X-Y plane and a cable which would be directly behind the aircraft. The lateral deflection is the added displacement caused by the wake. The 3-g turn deflects the endbody most in the lateral direction as depicted by Figure 5-15, while it also deflects most over the majority of the turn.

Most likely, the 3-g turn is experiencing the large amount of lateral deflection due to its larger turn radius, which causes the endbody and cable to spend more time in close proximity to the trailing wake from the wingtips. This is seen in Figure 5-16, where the induced wake velocity felt by the endbody is reported over the turn time for each load factor. As the figure shows, the 3-g turn is inducing the most wake at the endbody across the entire turn, whereas the 7-g and 5-g turns spike at the onset of the turn, when the endbody is still in close proximity to the trailing wake. The 7-g turn is executed so quickly that the endbody spends very little time in proximity to the trailing wake, therefore after the initial shock of the turn, it induces less velocity and deflects less later in the turn.
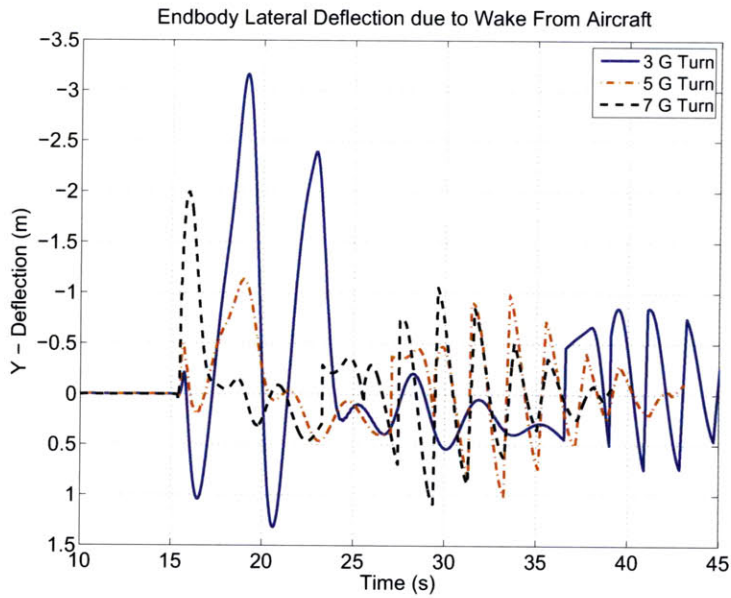
Figure 5-15: Endbody Deflection due to Wake Effects in the Y Direction During Varying Load Factor Turns with 50 m Steel Cable
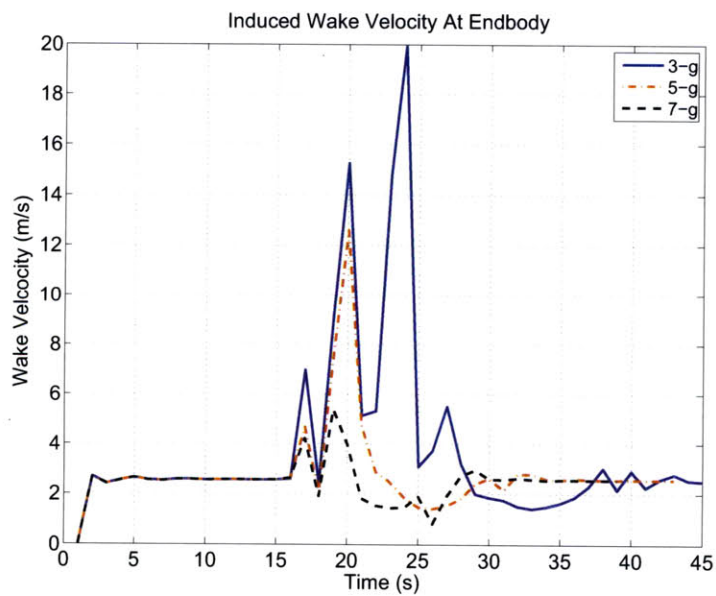

Figure 5-16: Induced Wake Velocity Felt by Endbody During Varying Load Factor Turns with 50 m Steel Cable

Figure 5-18 explains why the 7-g turn is experiencing the most displacement over all, as the largest spike in top of the cable induced velocity occurs in the 7-g case around $22\,m/s$ following onset of the turn, and nearly $65\,m/s$ at the mid cable point soon thereafter. Although it does not spend as much time in proximity to the wake, the sudden increase and maximum level spike occurring in the 7-g case causes it to oscillate and deflect the most overall. Figures 5-17 and 5-18 depict the induced velocity felt by the cable at the midpoint as well as aircraft attachment.

These figures show that the 7-g case does in fact impart more velocity than its counterparts due to its larger overall wake strength. The fact that the lateral deflection was most for the 3-g turn, however, may mean that wake velocity induced on the endbody is more of a determining factor in lateral cable shape and endbody deflection than the velocity imparted on the upper end of the cable. This is due to the endbody's drag force, which is higher than the cable drag because of its higher coefficient of drag, as well as the increased moment arm a force at the endbody end of the cable has when compared to a force at the top of the cable where it is pinned to the aircraft. Therefore, because more velocity is induced at the endbody end, the 3-g case deflects the most in the lateral direction as it spends more time in proximity to the trailing wake.
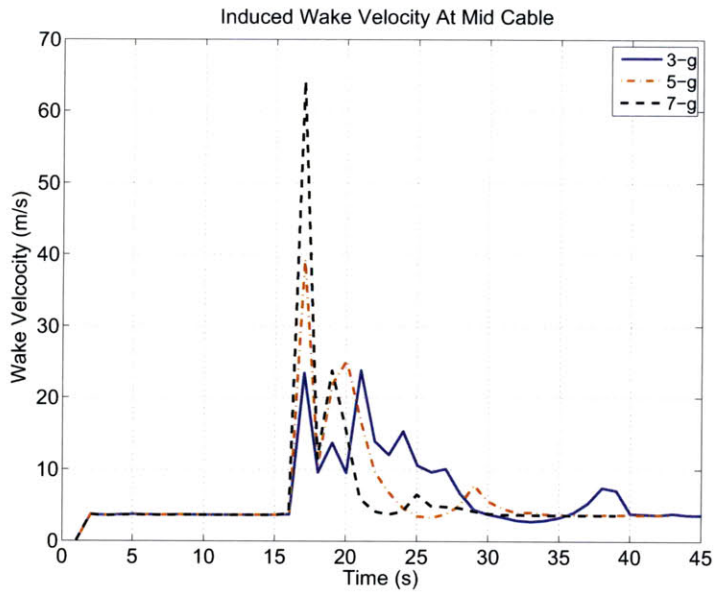
Figure 5-17: Induced Wake Velocity Felt by Mid Cable Segment During Varying Load Factor Turns with $50\,m$ Steel Cable
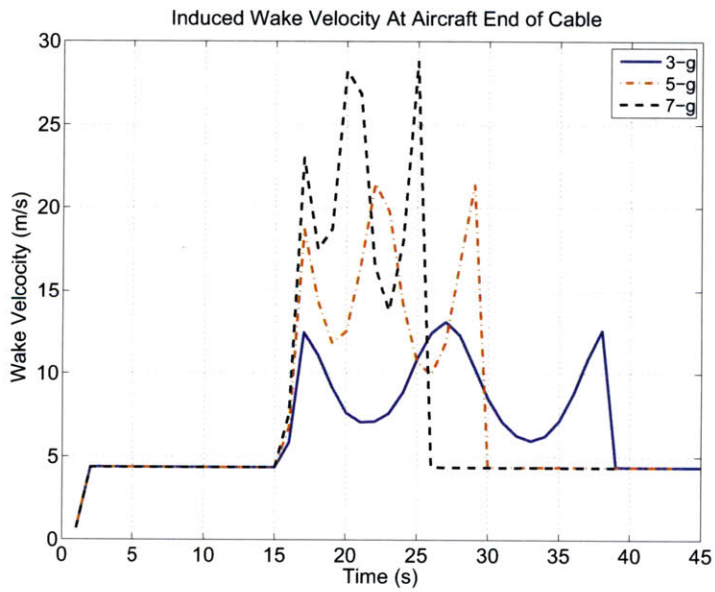

Figure 5-18: Induced Wake Velocity Felt by Aircraft End of Cable During Varying Load Factor Turns with $50\,m$ Steel Cable

87

Figure 5-19 depicts the situation which is occurring in the 3-g turn when the endbody oscillation begins. The figure depicts the overhead view of the system as it begins the banked turn to the left. Motion is occurring from the bottom right of the figure towards the top left of the figure. The left and right wingtips are marked, as well as the entire cable and endbody system. The trailing cable and endbody are passing through, or in close proximity, to the trailing wake. After the initial motion into the turn, the endbody returns to a position close to the trailing wake, which appears at the top left of the figure. Although this passing through occurs in all three load factor turns, the 3-g turn is occurring slower than the 7-g turn, therefore the passing through of the vortex is occurring over a longer time period. This allows the wake to impart more velocity on the lower load factor turn over the course of the turn despite the higher trailing wake in the 7-g case. Figure 5-20 depicts this, as the 7-g turn does not allow the endbody to return as close to the wake through the turn.
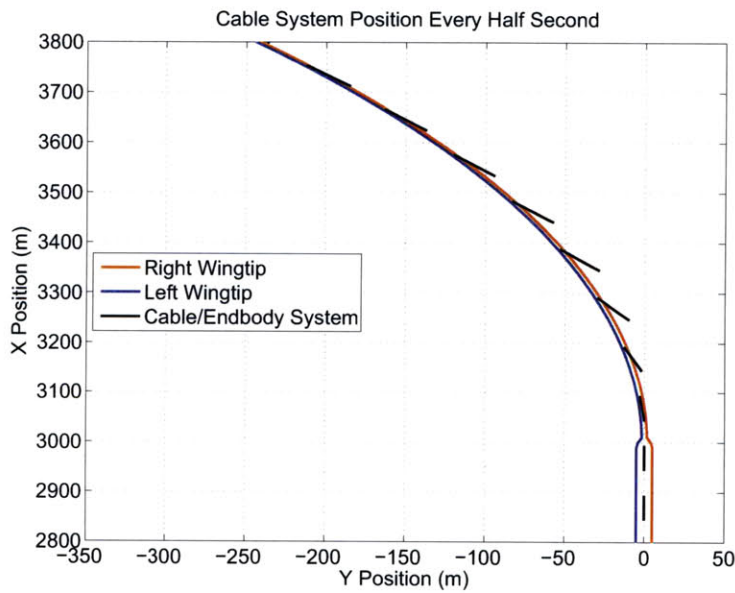

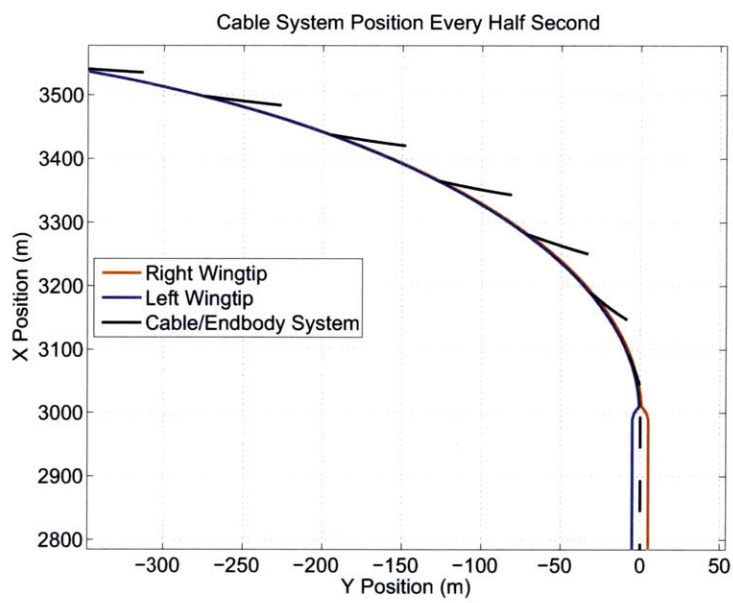Figure 5-19: Top Down View of 3-g Turn for 50 m Steel Cable

Figure 5-20: Top Down View of 7-g Turn for 50 m Steel Cable

The varying load factor turns were repeated for larger lengths, and the results were the same as the standard turn presented earlier. The larger cable lengths experienced minimal displacement, as seen in Figure 5-21. These are the results of the Kevlar turns conducted with $1\,km$ cables. The steel cables exhibited the same response, with little deflection due to the wake. Load factor had no impact for the longer cables, as the 7-g turn also experiences minimal deflection. The difference in response between the $50\,m$ to $1\,km$ cable is due to the increased inertia of the longer cables.

The shorter cables may also be affected more by the wake as it is closer to the actual endbody, the drag sphere, which exhibits more drag force than a cable segment. As Figure 5-19 shows, the drag sphere in the shorter cable lengths is passing through, or very near, the recently released portion of the right wingtip's trailing vortex. In a longer cable, the endbody is hanging lower in the Z-direction, therefore it would be further away from the trailing wake vortex to begin with. This appears in Figure 5-22, which shows the wake velocity induced at the endbody for a $1\,km$ cable, which is significantly smaller (note the y-axis label of $10^{-4}\,m/s$) than the $50\,m$ case shown above in Figure 5-16. The wake velocity induced at the cable portion nearest the aircraft is on the same order as the $50\,m$ case, however, the endbody effects are close to zero, and the $1\,km$ results show minimal endbody deflection as seen in Figure 5-21!
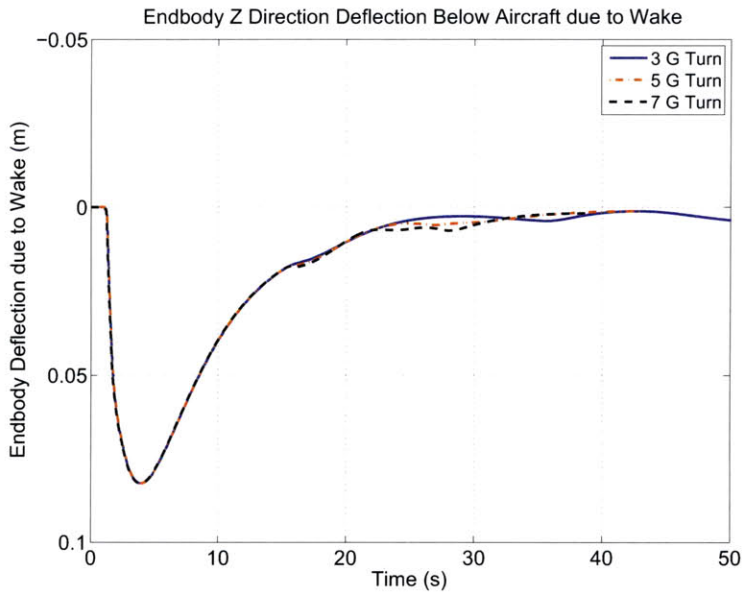
.

Figure 5-21: Endbody Deflection due to Wake Effects in the Z Direction During Turn Maneuver with Varying Load Factor of 1 km Kevlar Cable
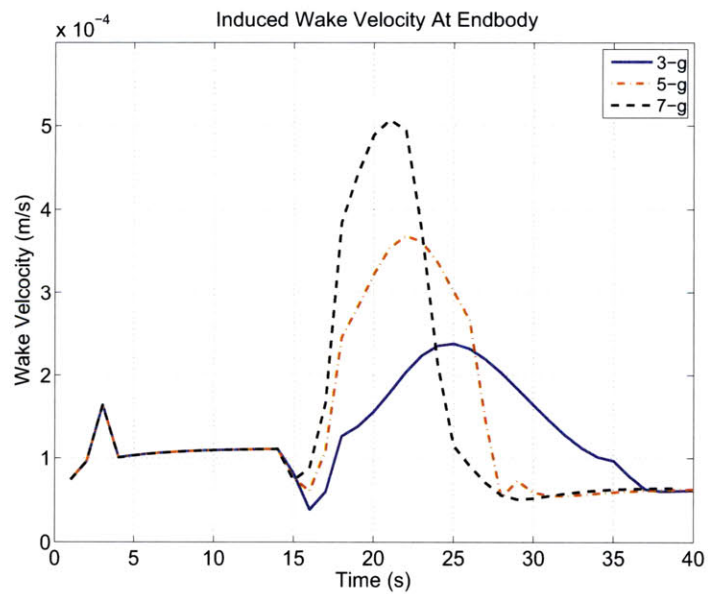

Figure 5-22: Induced Wake Velocity Felt by Endbody During Varying Load Factor Turns with 1000 m Steel Cable

5.4 Climb

The third maneuver analysis was conducted on an aircraft climbing in altitude. Two separate climbs were conducted where the aircraft pitched up to reach a new altitude and then nosed over to level flight once it reached the new height. The two climbs were conducted for $150\,m$ and $1500\,m$ of vertical gain. They were conducted with both Kevlar and steel cables, as well as varying cable lengths. Figure 5-23 shows the effects of wake on the two climbs with each cable material. The same pattern appears as in the other maneuvers where the longer cables seem unaffected by the wake while the shortest cable remains most affected. Also, the Kevlar cables were affected more by the addition of wake than steel cable with a maximum deflection of nearly 4% occurring for the $50\,m$ cables.
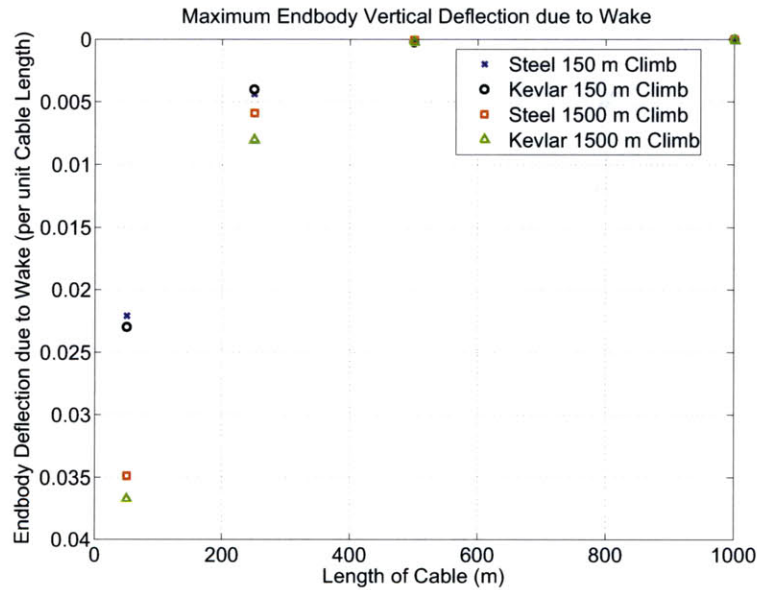

Figure 5-23: Endbody Deflection due to Wake Effects in the Z Direction During $150\,m$ and $1500\,m$ Climb Maneuvers with Varying Steel and Kevlar Cable Lengths

Also in Figure 5-23, the climb of 1500 m induces more wake effects on the cable. This is due to the greater load factor experienced by the aircraft during the maneuver than the shorter climb. Both climbs were conducted in the same time span, therefore the higher climb must perform a more violent pitch up maneuver to attain the correct amount of altitude in the allotted time. This more violent climb maneuver is shown in Figure 5-24, which depicts a 50 m steel cable example.

During the climb, the cable and endbody actually pass ahead of the aircraft and then snap back through the trailing wake. For comparison, the less violent 150 m climb is also shown in Figure 5-25. In the 150 m climb, the endbody remains below and behind the aircraft for almost the entire maneuver, never passing above or in front. The figure's scaling produces the appearance of cable shortening, which is not the case. Longer cables exhibit the same response even for the more violent climb. This is seen in Figure 5-26, which shows the 1 km steel cable enduring the same violent climb maneuver. The cable remains behind and below the aircraft throughout the entire maneuver, and only alters shape when the aircraft is leveling off following the overshoot.
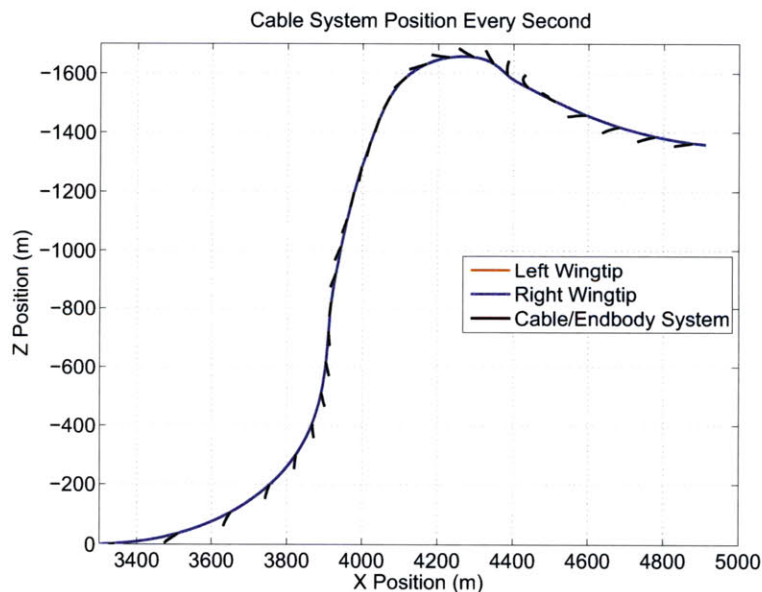

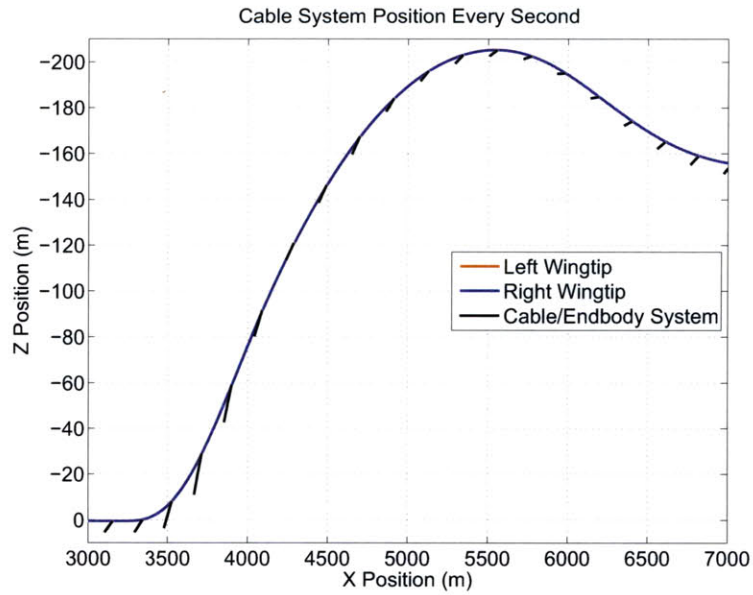Figure 5-24: Cable Shape during 1500 m Climb Maneuver, 50 m Steel Cable

Figure 5-25: Cable Shape During $150\,m$ Climb Maneuver, $50\,m$ Steel Cable

Figure 5-26: Cable Shape During $1500\,m$ Climb Maneuver, $1000\,m$ Steel Cable

At three points in the violent climb there are sizeable deflections, as seen in Figure 5-27. The first major deflection occurs right after the aircraft pitches up to begin the climb. The endbody is not directly in the trailing wake, but the wake strength is significantly increasing as the aircraft's load factor increases while it attains a higher pitch angle. As you can see in Figure 5-28, the cable and endbody system is dealing with the higher wake strength as well as the new aircraft attitude, causing extra interaction with the trailing wake.
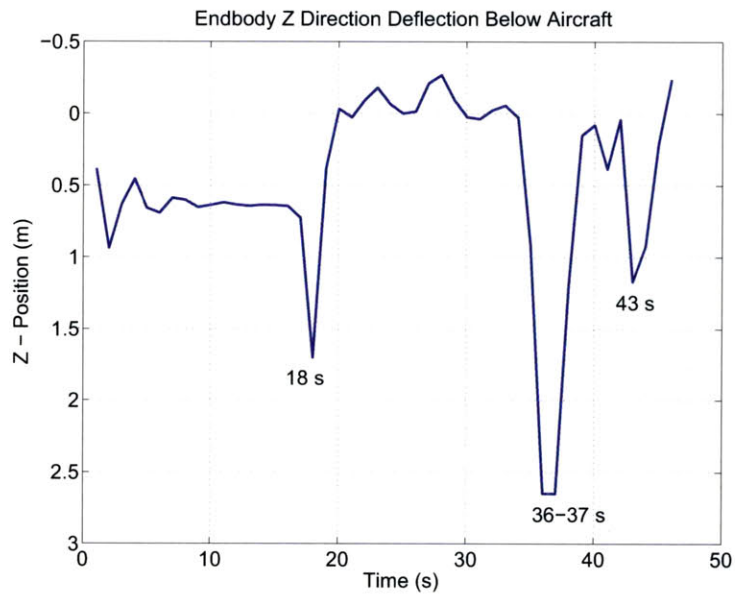

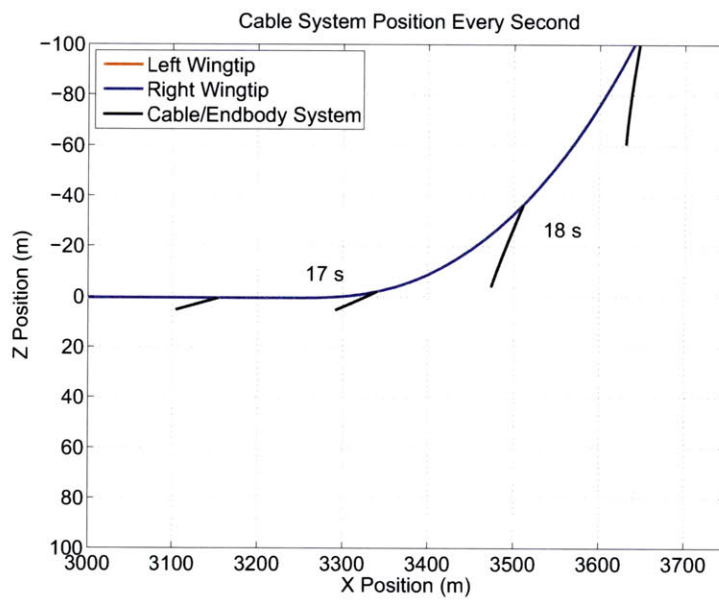Figure 5-27: Z-Deflection of Endbody during 1500 m Climb Maneuver, 50 m Steel Cable

Figure 5-28: Cable Shape during $1500\,m$ Climb Maneuver, $50\,m$ Steel Cable, around Time $= 18\,s$

The second major endbody deflection occurs around the time of 36 seconds, seen in Figure 5-29. At this time, the aircraft is beginning to nose over back to its original pitch angle. During this process, the wake strength is reducing as the aircraft drops load factor. However, the endbody and cable system are passing directly through the trailing wake, which would cause the spike in deflection.

The third major event occurs around 43 seconds. At this time, in Figure 5-30, the wake is actually causing the endbody to place higher in altitude than it would without a wake. This is the result of an oscillation that does not occur in a wake-less example. The endbody is reacting to the aircraft nosing over and decreasing altitude as it overshoots its intended altitude. The system is dealing with decreased wake strength, as well as a diving aircraft, and their interaction combined with the previous time step's motion provides energy for oscillation in the system. Between the timesteps of 42 seconds and 43 seconds the cable is also crossing the path of the trailing wake. The induced wake velocity throughout the climb is cataloged in Figure 5-31. As the figure shows, the induced wake velocity is spiking at the same three points in time that major deflections are occurring.
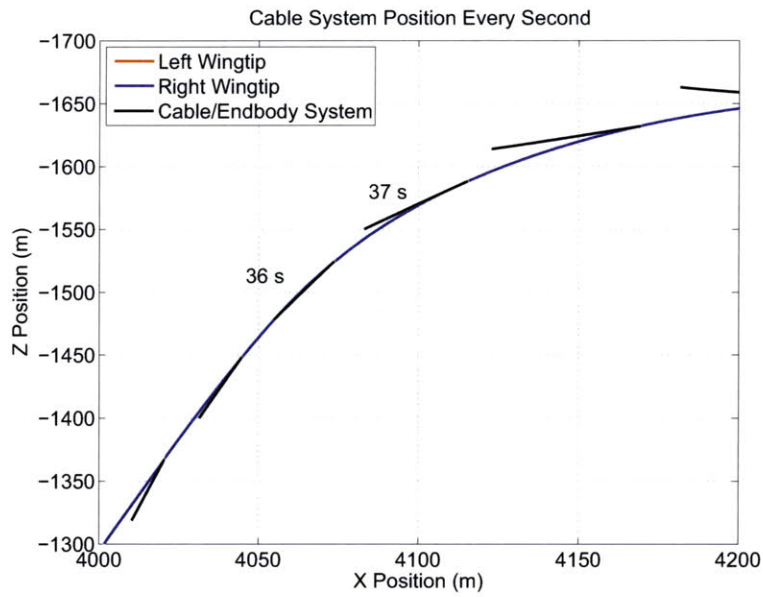
Figure 5-29: Cable Shape during $1500\,m$ Climb Maneuver, $50\,m$ Steel Cable, around Time $= 36\,s$
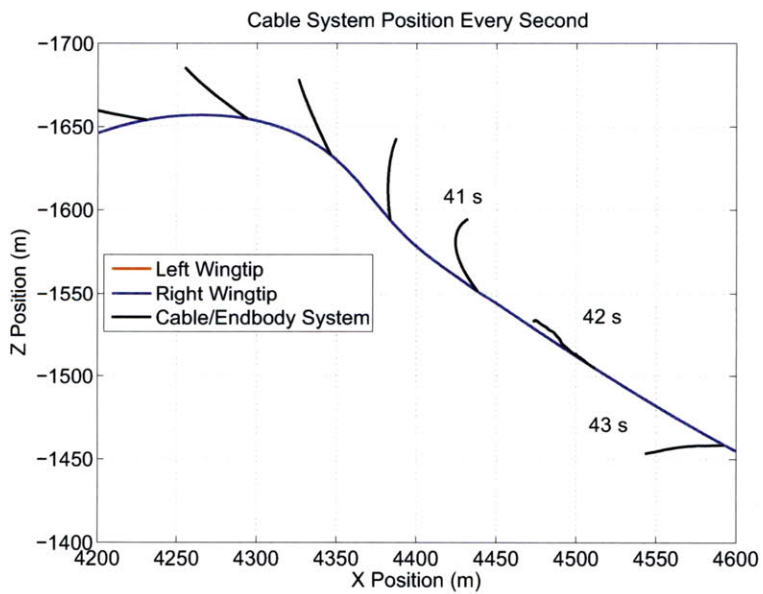

Figure 5-30: Cable Shape during $1500\,m$ Climb Maneuver, $50\,m$ Steel Cable, around Time $= 43\,s$
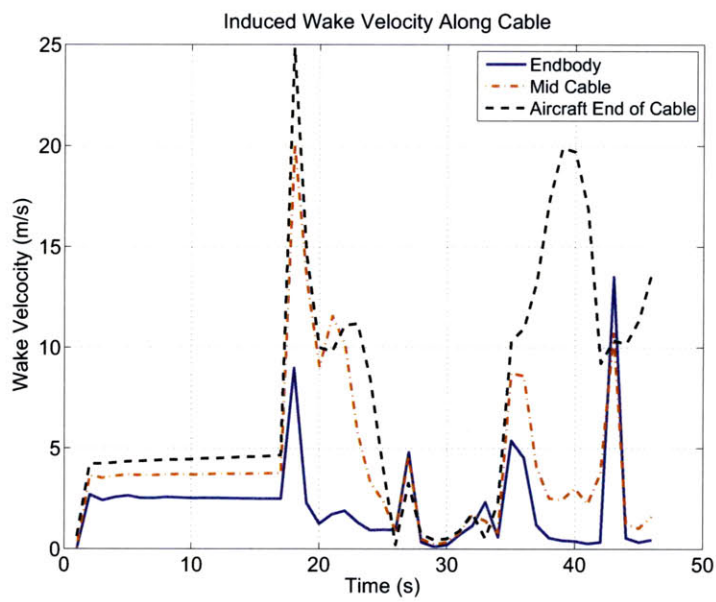
Figure 5-31: Induced Wake Velocity Felt by Cable during 1500 m Climb Maneuver, 50 m Steel Cable

Chapter 6

Conclusions and Recommendations

6.1   Conclusions

The primary objectives of this thesis were to create a six degree of freedom cable and endbody system model, subject the model to maneuvers, and incorporate aircraft wake effects in order to analyze characteristics such as endbody placement and system shape. The main objectives were accomplished, as shown in the previous chapters. Overall, incorporating wake effects into a maneuvering cable-endbody system is proven to be achievable without excessive computational resources. Although the model produced is not as detailed or as complex as possible, it is a good starting point for further research, and provides dynamical feedback to generate results sufficient for analysis.

The results show that the estimated wake generated by a light, tactical aircraft affected the cable endbody system minimally for longer cable lengths. Cable lengths between $500\ m$ and $2\ km$ experience a negligible difference in endbody and cable position with the addition of induced wake velocities. This minimized effect is most likely due to the increased mass and inertia of such longer cables, as well as decreased induced wake velocities at the endbody. The minimal effects were exhibited through all three maneuvers for the lengthy cables.

The trailing wake, however, had an affect of around $8\ m$ deflection for shorter cable lengths, especially during maneuvering flight. The most deflection occurs for a

7-g level turn conducted by a light tactical aircraft. In this turn, the endbody passes directly through the trailing wake following a sudden increase in load factor. This causes a deflection of around 8 m for a 50 m steel cable. When taking into account the entire time period, the endbody is displaced more on average by the lower load factor turn of 3-g's. This is most likely due to its larger turn radius, which allows the endbody to remain within close proximity of the trailing wake, unlike the higher load factor turns where the aircraft is changing heading rapidly.

Also appearing in the results, is that certain combinations of cable properties and aircraft motion produce endbody placement ahead of the aircraft. Violent climb maneuvers conducted with a 50 m cable, both steel and Kevlar, cause the endbody to pass ahead of the aircraft during the initial aircraft pitch up. Such effects can complicate many scenarios for cable endbody systems such as aerial refueling or towing decoys.

The results show the minimal difference between reactions of cables comprised of Kevlar or Steel. Although Kevlar cables have a lower modulus value, about a third of the steel, and a fifth of their density, their reactions mimicked the steel cables with minor differences. In steady state conditions, the Kevlar cables were positioned above steel cables, as their lower mass lead to a smaller gravitational force. During maneuvers, Kevlar cables deflected slightly more with the addition of wake forces, also due to their lower mass.

6.2 Recommendations

Although the primary goals of the thesis were met, there are still areas of the research which should be pursued in the future. In this study, the endbody was modeled as a simple drag sphere. As was shown in Chapter 2, various endbodies exist throughout the world that are not relegated to simple drag spheres such as maneuverable instruments and even other aircraft. In order to better characterize endbody motion and placement due to wake and maneuvers, accurately detailed endbodies should be used for more specific purposes.

Along with endbodies, more specific aircraft should be used in order to generate accurate wake data. The research in this thesis relied on the same generic tactical sized aircraft for all results for standardization and non dimensionalization purposes. All manners of aircraft tow objects, such as decoys or targets, and their wake may be substantially different than the aircraft used herein, such as the wake from a cargo aircraft maneuvering at low altitudes.

If the generic tactical aircraft is to be pursued for more detail, it is also recommended to generate more complex and accurate maneuvers. Many of the maneuvers presented in this thesis are basic turns, whereas cable towed endbody systems will be subjected to much more violent maneuvers, especially in combat scenarios. These maneuvers will also produce different wake fields, which could affect endbody position in a more serious manner.

Lastly, if time isn't an issue, it is recommended to enhance the wake modeling process through a more complex process such as computational fluid dynamics. Wake fields generated through this process would represent a more detailed analysis of those produced by aircraft during maneuvers. The wake fields generated in this thesis were based on a solid mathematical foundation, however, simplifications were made using assumptions that may not be needed when using computational fluid dynamics. In reality, the aircraft wake is not rolled into only two trailing wake vortices, and things such as a jet plume of engine exhaust may also be present in affecting cable endbody systems. Along with re-coding the wake process, it is recommended to write the entire cable system code in C++, as opposed to a combination of Matlab and C++, in order to address time and computational resources in a more efficient manner.

Bibliography

[1] J. Bertin and R. Cummings. *Aerodynamics for Engineers*. Prentice Hall, Upper Saddle River, New Jersey, fifth edition, 2009.

[2] Y. Choo and M. Casarella. A survey of analytical methods for dynamic simulation of cable-body systems. *Journal of Hydronautics*, 7(4):137–144, October 1973.

[3] USN ENS C. Hill. Theoretical modeling of the transient effects of a towline using the method of characteristics. Master's thesis, Air Force Institute of Technology, 2006.

[4] USN ENS T. Richardson. Parametric study of the towline shape of an aircraft decoy. Master's thesis, Air Force Institute of Technology, 2005.

[5] B. Etkin. Stability of a towed body. *Journal of Aircraft*, 35(2):197–205, 1998.

[6] J. Genin and T. Cannon. Equilibrium configuration and tensions of a flexible cable in a uniform flowfield. *Journal of Aircraft*, 4(3):200–202, 1967.

[7] H. Glauert. The form of a heavy cable used for towing a heavy body below an aeroplane. R and M 1592, Aeronautical Research Committee, 1934.

[8] S. Hoerner. *Fluid-Dynamic Drag*. Hoerner Fluid Dynamics, Brick Town, New Jersey, first edition, 1965.

[9] R. Huffman and J. Genin. The dynamical behaviour of a flexible cable in a uniform flow field. *The Aeronautical Quarterly*, 22:183–195, 1971.

[10] J. Anderson Jr. *Fundamentals of Aerodynamics*. McGraw Hill, New York, New York, third edition, 2001.

[11] J. Cochran Jr., M. Innocenti, T. No, and A. Thukral. Dynamics and control of maneuverable towed flight vehicles. *Journal of Guidance, Controld, and Dynamics*, 15(5):1245–1252, 1992.

[12] L. Karlsen. Large scale dynamics of long flexible cables towed through air. KTH Aero TN 61, Royal Institute of Technology Department of Aeronautical Engineering, Stockholm, Sweden, 1981.

[13] E.J. Kelly. Analysis and simulation of cable/endbody motion. Project Report MTCD-7, Lincoln Laboratory - Massachusetts Institute of Technology, Lexington, MA, 1998.

[14] J.R. Lehn. Research and development program for airborne towed vehicles. Technical report, Naval Air Development Center, Warminster PA, 1963.

[15] E. Magat. Fibres from extended chain aromatic polyamides. *Philosophical Transactions of the Royal Society of London. Series A, Mathematical and Physical Sciences*, 294(1411):463–472, January 1980.

[16] C. Matuk. Stress in a towing wire due to accelerations of the towing vehicle. T 33, University of Sweden Department of Mechanical Engineering, 1979.

[17] B. Nagabhushan and E. Cliff. Maneuver stability of a vehicle with a towed body. In *AIAA Atmospheric Flight Mechanics Conference*. AIAA, August 1982.

[18] N. Nakagawa and A. Obata. Longitudinal stability analysis of aerial-towed systems. *Journal of Aircraft*, 29(6):978–985, 1992.

[19] S. Norris and D. Andrisani. Longitudinal equilibrium solutions for towed aircraft and tow cable. In *AIAA Atmospheric Flight Mechanics Conference*. AIAA, August 2001.

[20] D. Pierce and L.J. Beecham. Some aerodynamic considerations of the flight characteristics of towing systems using long towlines at high speeds. CP 1235, Royal Aircraft Establishment, 1972.

[21] J. Quiesenberry and A. Arena. Dynamic simulation of low altitdue aerial tow systems. In *AIAA Atmospheric Flight Mechanics Conference*. AIAA, August 2004.

[22] J. Quiesenberry and A. Arena. Discrete cable modeling and dynamic analysis. In *AIAA Aerospace Sciences Meeting and Exhibit*. AIAA, January 2006.

[23] R. Bollard R. Holler, J. Brett. The use of kevlar for small diameter electromechanical marine cables. In *Proc. 1975 IEEE Oceans Conference*, pages 169–173, San Diego, 1975.

[24] Raytheon Space and Airborne Systems, Goleta, California. *AN/ALE-50 Towed Decoy System*. http://www.raytheon.com/capabilities/products/ale50/.

[25] P. Williams, D. Sgarioto, and P. Trivailo. Optimal control of an aircraft-towed flexible cable system. *Journal of Guidance, Control, and Dynamics*, 29(2):401–409, 2006.

[26] Z.H. Zhu and S. A. Meguid. Elastodynamic analysis of aerial refueling hose using curved beam element. *AIAA Journal*, 44(6):1317–1324, June 2006.

[27] Z.H. Zhu and S. A. Meguid. Modeling and simulation of aerial refueling by finite element method. *International Journal of Solids and Structures*, 44:8057–8073, June 2007.

[28] Z.H. Zhu, S. A. Meguid, and L. Ong. Dynamic multiscale simulation of towed cable and body. In *Second MIT Conference on Computational Fluid and Solid Mechanics*, pages 800–803. Massachusetts Institute of Technology, 2003.